PERKIN ELMER
Government Systems Sector

PR B11-0064

Project Report

IMAGING PHASED TELESCOPE ARRAY STUDY

A FINAL STUDY REPORT

Prepared by:

James E. Harvey

The Perkin-Elmer Corporation
Electro-Optical Technology Division
100 Wooster Hts. Rd., M/S 813
Danbury, Connecticut 06810

January 15, 1989

Prepared For:

The NASA Marshall Space Flight Center

NASA Contract NAS8-36105

TABLE OF CONTENTS

TABLE OF CONTENTS (Cont.)

1.0 PREFACE

This study is an Air Force funded extension of the NASA Astronomical Interferometric System Technology Requirements (AISTR) Study whose broad objective was to advance the technical and scientific endeavors of our nation in space astronomy. The Air Force Weapons Laboratory (AFWL/ARBB) has initiated an aggressive advanced imaging development effort under the auspices of the Air Force FORCAST II PT-49 technology initiative. PT-49 is a three year program to develop and apply those advanced electronic and optical imaging technologies which support Air Force missions. This study incorporates and extends the results of related NASA work in the area of imaging phased telescope arrays into the PT-49 program and will augment the AFWL in-house experimental phased array optical imaging initiative now underway.

The study was accomplished under sponsorship of the Office of Aeronautics and Space Technology, NASA Headquarters and directed through the Program Development Directorate of NASA's Marshall Space Flight Center (MSFC). Technical direction for this study came from Dr. Christopher DeHainaut and Dr. Lawrence Weaver at the Air Force Weapons Laboratory (AFWL). Grateful acknowledgement is made to Mr. Max Nein of MSFC and Dr. Janet Fender of AFWL whose efforts made this cooperative inter-agency study possible.

The principle investigator of this study at Perkin-Elmer was Dr. James E. Harvey and he was assisted by Dr. Christ Ftaclas in performing analyses and making image quality predictions. Michael Krim, Richard Rockwell and Alan Wissinger participated heavily in the earlier phases of this contract and many useful discussions with Bruce Boyce, Harold Levenstein, Dr. Paul Reid, and Dr. Roderick Scott are gratefully acknowledged.

Comments and requests for additional copies of this report should be referred to Mr. Max Nein at the Marshall Space Flight Center or to Dr. Christopher DeHainaut at the Air Force Weapons Laboratory.

2.0 INTRODUCTION

Previous studies have indicated that pupil mapping errors and the off-axis aberrations of the individual telescopes of a phased telescope array can rapidly degrade image quality for increasing field angles thus severely limiting the useful field-of-view of the phased telescope array.[1-5] Correcting the pupil mapping errors poses a severe engineering challenge, but the residual design aberrations of the individual telescopes is more fundamental in nature.

The results of preliminary calculations performed in Reference 5 indicate that for visible light and 2.0 meter diameter subapertures, either of the above error sources may limit the useful field-of-view to a few tens of arc seconds for some subaperture configurations of interest.

These preliminary indications of severe field-of-view limitations of phased telescope arrays provided the impetus for the current parametric study.

2.1 OBJECTIVE

The objective of this effort is to perform parametric trade studies and sensitivity analyses allowing us to predict the optical requirements for phased telescope arrays for imaging applications requiring a substantial field-of-view (FOV). The product of this effort is a better understanding of the inter-relationship between various optical, mechanical, and scenario-dependent parameters affecting imaging phased telescope array system performance. This understanding allows design methodologies to be developed and tolerances to be derived for achieving desired image quality requirements over a specified FOV.

2.2 SCOPE

In order to determine the utility of phased telescope arrays to wide FOV applications, the sensitivity of various system and subsystem parameters to image quality must be known. This involved an understanding of the effects of aperture configuration (including the fill factor or dilution ratio), individual telescope configuration, beam combining techniques, residual optical design errors (particularly off-axis aberrations), optical fabrication tolerancing, mechanical tolerancing in the assembly and alignment process, pupil mapping and stability, sensing and control techniques and their effects upon overall system image quality. An error budget tree was thus developed to include optical design errors, optical fabrication errors, assembly and alignment errors, and environmental errors. Parametric analyses and trade studies allow the derivation of design and engineering tolerances from error budget allocations based upon known state-of-the-art performance characteristics. This error budget tree is therefore a mechanism for evaluating different telescope and subaperture configurations, beam train architectures, and control system concepts to predict, to the extent possible, the field-of-view limitations of phased telescope array imaging systems. The analysis is performed in sufficient depth to allow specification of system tolerances from given image quality requirements.

2.3 TECHNICAL APPROACH

It was emphasized by AFWL that they did not want us to merely evaluate a point design; hence, the technical approach was to perform parametric analyses and trade studies of the dominant error sources for a variety of telescope and subaperture configurations to determine their field-of-view limitations, then proceed to the next design in a hierarchy of telescope configurations with increasing degrees of freedom until the desired field-of-view was obtained in the telescope sizes of interest. Allowable error budget allocations were determined not only for residual design aberrations but for optical fabrication and alignment errors as well. In this manner we derived the resulting design and engineering tolerances and their scaling behavior for imaging phased telescope arrays.

2.4 STUDY TASKS

The five subtasks identified for this study are:

- Definition of System Issues
- Development of Error Budget Tree and Preliminary Allocations
- Parametric Trade Studies, Sensitivity Analyses, and Scaling Behavior
- Optical Performance Requirements and Derivation of Necessary Tolerances
- Program Management

In addition to discussing each of these subtasks, we review previous relevant work and model the AFWL Multipurpose Multiple Telescope Testbed (MMTT) to make image quality predictions as a function of field angle for this laboratory experiment and scaled-up versions of its basic design.

3.0 DEFINITION OF SYSTEM ISSUES

Although the objective of this study is to perform parametric trade studies and sensitivity analyses allowing us to predict the optical requirements for phased telescope arrays for imaging applications requiring a substantial field-of-view, system issues that need some initial definition in order to bound the problem are: image quality criterion, operating wavelength and spectral range, desirable field-of-view, aperture configuration, and individual telescope configuration. A strawman design is required for deriving quantitative tolerances. Variations from the strawman design have been evaluated as part of the analysis.

3.1 IMAGE QUALITY CRITERION

There has long been a desire to come up with a simple single-number merit function for characterizing the image quality of optical systems. Some frequently used image quality criteria are resolution [full-width at half-maximum (FWHM) of the point spread function (PSF)], Strehl ratio, rms wavefront error, fractional encircled energy, and a variety of modulation transfer function (MTF) characteristics. Since the point spread function is the squared modulus of the Fourier transform of the complex pupil function, the autocorrelation theorem theory allows us to define the optical transfer function as the normalized autocorrelation of the complex pupil function and to draw the relationship illustrated in Figure 3-1.[6]

The complex pupil function describes the wavefront aberrations that degrade image quality and, furthermore, these wavefront aberrations are rendered observable and measurable by interferometric techniques. Single-number merit functions derivable from interferometric data include the rms wavefront error and the peak-to-valley wavefront error. The amplitude spread function is not an observable quantity with ordinary sensors. The PSF is the irradiance distribution making up the image of an ideal point source.[7] Frequently used single-number merit functions obtained from the PSF are the resolution, Strehl ratio, and the fractional encircled energy. Encircled energy is a particularly relevant for expressing the optical performance of an optical system whose purpose is to collect light and direct it through the entrance slit of a spectrometer. The OTF contains all of the information about the spatial frequency content of the image. Limiting resolution and the transfer factor at a specific spatial frequency are single-number merit functions derivable from the OTF.

The proper criterion for evaluating optical performance depends upon a number of different factors: the nature of the source or object to be imaged, the nature of the detector or sensor to be used, and the goal of the particular application. For simplicity we will use Strehl ratio as the image quality criterion of choice in this study. Since we are interested primarily in the degradation of image quality with field angle for phased telescope arrays, the particular image quality criterion is of less concern than its variation with field angle. We fully recognize that for imaging applications where fine detail in extended objects is of concern, some characteristic of the MTF is a more appropriate performance criterion than Strehl ratio.

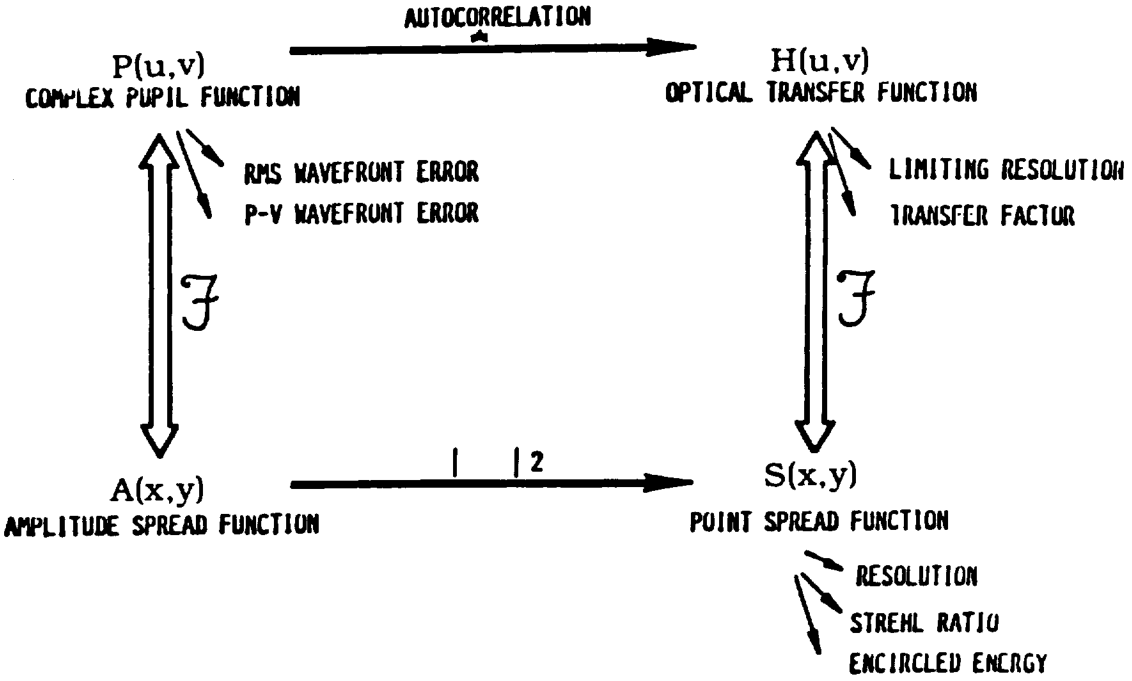

Figure 3-1. Some frequently used image quality criteria are properties of the complex pupil function. Others are obtained from the PSF or OTF. This figure shows the relationship between some of these different image quality criteria.

3.2 OPERATING WAVELENGTH AND SPECTRAL RANGE

Applications involving monochromatic imaging with active illumination as well as applications of broad-band (white light) imaging with phased telescope arrays are of interest. Wavelength has been treated as a study parameter; however, since some parameters must be held constant to keep the volume of data at a manageable level, the a nominal value of 0.5 µm has been chosen for calculating quantitative results in this report. Calculating polychromatic image quality is a straightforward extension of the calculations performed in this study.

3.3 DESIRABLE FIELD-OF-VIEW (FOV)

The Air Force Weapons Laboratory has considerable experience in optical phased telescope array technology for beam directing applications (zero-field systems).[8-12] They are currently building a Multipurpose Multiple Telescope Testbed (MMTT) which will be used for various imaging experiments.[13-14] A substantial FOV is desirable for some applications. We will investigate image quality parametrically as a function of FOV for various aperture configurations and telescope configurations. Break points between designs or configurations and their size scale will be identified. The nominal field-of-view requirement or goal has been taken as fifteen (15) minutes of arc. This corresponds to a full field of 0.5 degrees.

3.4 SUBAPERTURE CONFIGURATION

The choice of subaperture configuration can drastically affect the diffraction-limited imaging characteristics of a phased telescope array.[15] The images may contain artifacts and spurious images which are undesirable for certain applications involving point sources. Also if direct imaging phased telescope arrays are to be used for applications where it is necessary to study fine detail in extended objects, the subaperture configuration must not be so dilute as to produce substantial areas of zero modulation within the cut-off frequency of the MTF plane.[16] This topic is discussed in detail by the author in Reference 16 which is attached as Appendix A.

Since quantitative image quality predictions depend upon a specific subaperture configuration and this is not easy to vary parametrically, we needed some initial definition of the number, size, shape and position of subapertures making up the array. An appropriate number of individual telescopes making up an array, for the purposes of this study, is assumed to be between four (4) and twelve (12). Several strawman configurations made up of circular subapertures (which could easily be refined to be annulii) whose diameters are varied parametrically were thus evaluated in this study.

Figure 3-2 illustrates: 1) an arrangement of four subapertures similar to the configuration of the National New Technology Telescope (NNTT) being planned by NOAO and the MMTT at AFWL, 2) six subapertures similar to the Multiple Mirror Telescope operated by AURA on Mt. Hopkins south of Tucson, Arizona, 3) a two-dimensional nonredundant array of six subapertures referred to as a Golay-6 configuration,[17] 4) a Circle-N configuration where N is any desired number (most likely 7, 9, or 11), 5) another two-dimensional nonredundant array of nine subapertures referred to as a Golay-9 configuration, and 6) an eight-element Mill's Cross consisting of two orthogonal one-dimensional nonredundant arrays of four subapertures each.

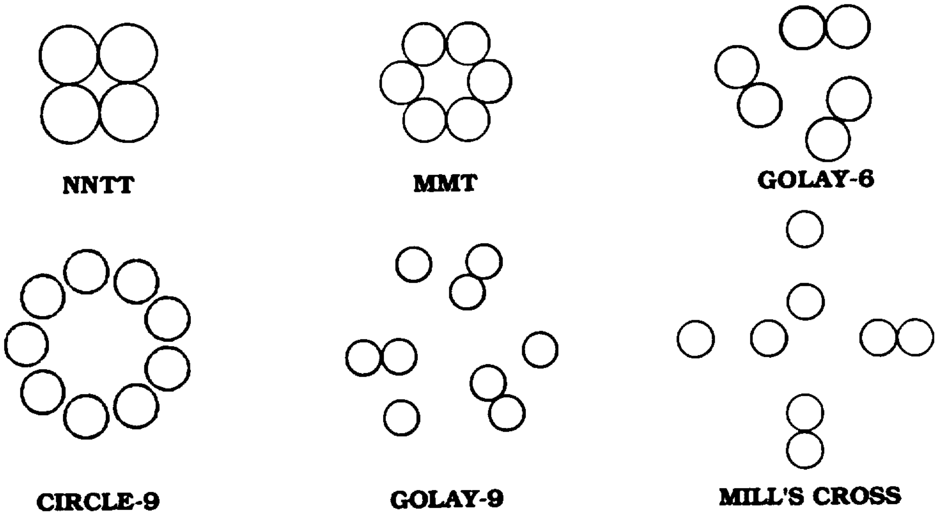

Figure 3-2. Subaperture configurations considered in this study.

The dilution ratio (ratio of the separation of adjacent subapertures to their diameter) of the array is also a study parameter. It should be noted that compact two-dimensional arrays are desirable for continuous coverage in the u-v (MTF) plane as illustrated in Figure 3-3. A dilution ratio greater than two (2) will assure the existence of areas of zero modulation in the MTF.

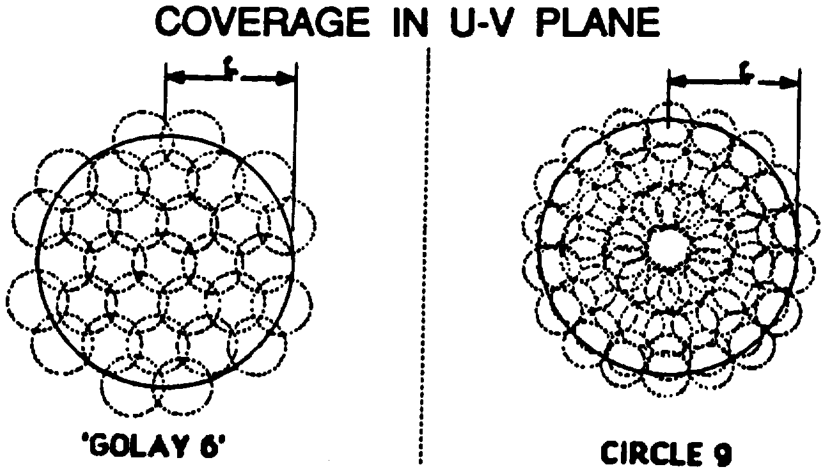

Figure 3-3. Compact two-dimensional arrays provide continuous coverage in the u-v (MTF) plane. This is desirable if fine detail is to be observed in extended objects.

3.5 INDIVIDUAL TELESCOPE CONFIGURATION

Synthetic aperture telescopes fall into two generic types; those consisting of a segmented primary mirror (perhaps substantially thinned or diluted) with a common secondary mirror as shown schematically in Figure 3-4, and those made up of an array of independent telescopes whose images are then combined and phased with appropriate optics as shown schematically in Figure 3-5.

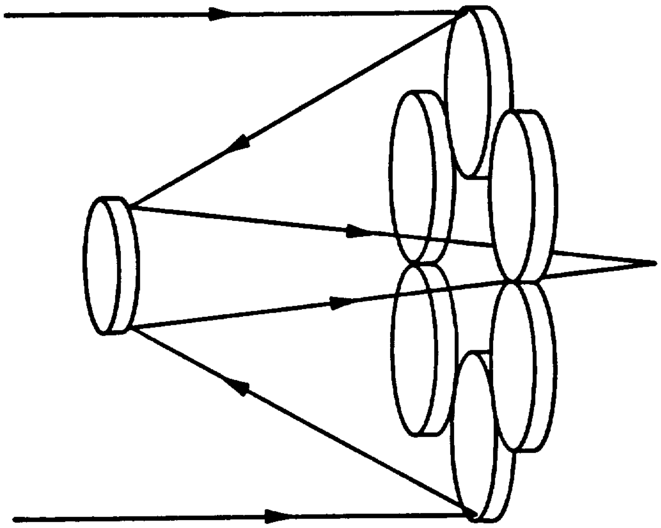

Figure 3-4. Synthetic aperture telescope consisting of a segmented primary mirror and a common secondary mirror.

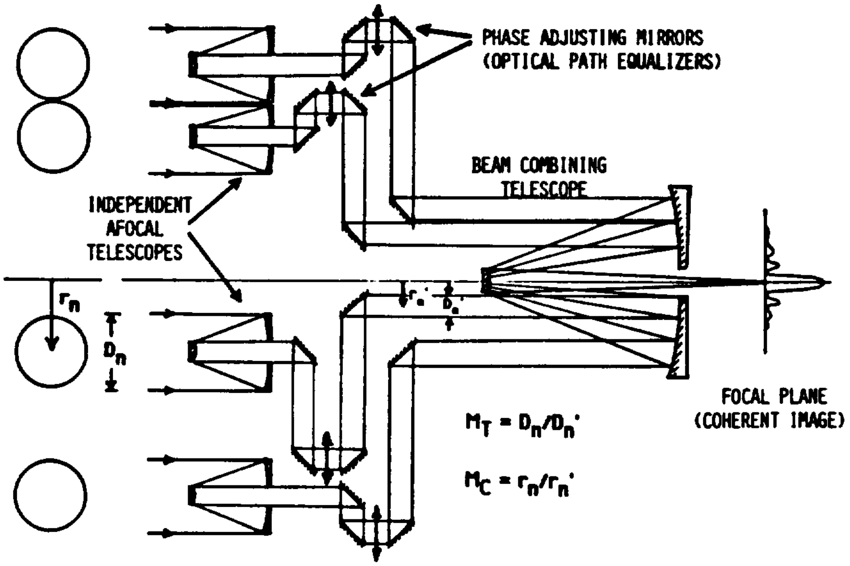

Figure 3-5. Configuration for a phased array of afocal telescopes complete with phase adjusting mirrors and beam combining telescope.

There are important considerations to be made concerning fabrication, assembly, alignment, deployment, and performance when choosing one type over the other for a large space telescope. Some of the trade-offs were studied in an earlier phase of this contract.[18] The modular aspect of phased arrays of independent telescopes should provide substantial advantages in the construction of a large telescope in space since each individual telescope can be fabricated, assembled, and aligned on the ground. The complete module can then be launched into orbit and fitted into the array thus minimizing the necessary amount of on-orbit assembly. However, field-of-view limitations are much more severe for this type of synthetic aperture imaging system than for the more conventional system that has a segmented primary mirror and a common secondary mirror.

In this study we will limit our attention to phased arrays of identical independent telescopes and employ a systems engineering approach to determine quantitatively the field-of-view limitations of such arrays as they are scaled up in size for imaging applications in space. A nominal goal for the field-of-view will be 0.5 degrees.

An error budget tree will be developed which includes optical design errors (aberrations of the individual telescopes), optical fabrication errors (including both optical surface figure and finish errors), assembly and alignment errors (including both errors within the individual telescopes, and errors between the individual telescopes), and finally, environmental errors such as vibration-induced image jitter, image degradation due to thermally-induced drift and deformations, gravity release errors, etc. We will start with an array of two-mirror afocal telescopes of the Mersenne design (confocal paraboloids) as shown schematically in Figure 3-5 which are inherently free of third-order spherical aberration, third-order coma, and third-order astigmatism. We will then identify a hierarchy of telescope configurations with increasing degrees of freedom to compensate dominant error sources such as the field curvature of the individual telescopes, magnification errors between the individual telescopes, and the control of both lateral and axial pupil mapping errors.

4.0 REVIEW OF PREVIOUS RELEVENT WORK

In addition to the obvious requirement to precisely phase the individual telescopes making up the array, two separate mechanisms known to further degrade the image of off-axis object points while the array remains phased upon an on-axis object point are pupil mapping errors and the field curvature of the individual telescopes. The pupil mapping errors can be broken down into lateral and axial pupil mapping errors. A brief review of previous work dealing with these dominant error sources will be presented here.

4.1 PISTON AND TILT ERRORS

R. R. Butts of the Air Force Weapons Laboratory (AFWL) has performed a rather exhaustive study of the relative peak intensity as a function of rms piston and rms tilt errors for different numbers of subapertures.[19] The results of the study are shown Figure 4-1 for six subapertures arranged in the MMT configuration. Note that the peak intensity or Strehl ratio is about three (3) times more sensitive to rms piston errors than rms tilt errors.

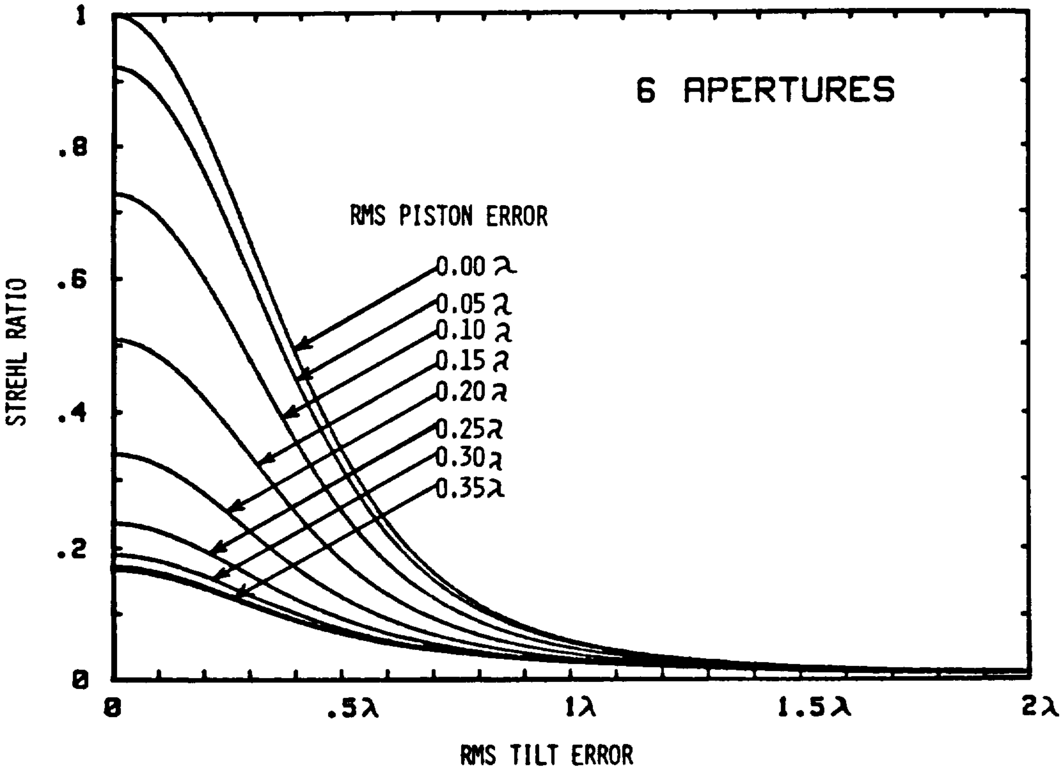

Figure 4-1. Strehl ratio vs. rms tilt errors for different values of rms piston error for the MMT configuration of six subapertures.

4.2 LATERAL PUPIL MAPPING ERRORS

It has been recognized by a variety of investigators that the exit pupil geometry must be precisely matched to the entrance pupil geometry of phased telescope arrays if a significant field-of-view is to be achieved.[1-5]

The exit pupil of an optical system is by definition an image of the entrance pupil formed by the optical system. For conventional imaging systems the exit pupil is thus automatically an exact scaled replica of the entrance pupil. However, for a multi-axis telescope array with a variety of folding mirrors in each separate optical path such as that illustrated in Figure 3-5, this condition is not automatically satisfied, but must be satisfied by deliberately and precisely positioning the final folding mirror directing the individual beams into the beam combining telescope.

Imaging phased telescope arrays can thus be described as a two-step process as illustrated in Figure 4-2. First, there is a pupil mapping process in which the entrance pupil of the array (made up of the primary mirrors of the independent telescopes) must be mapped into the exit pupil plane of the beam combining telescope. Then there is a Fourier transform process in which the image characteristics are determined from this system pupil function. If high image quality is to be achieved over any significant field-of-view, the pupil mapping process must be performed such that the exit pupil is an exact (scaled) replica of the entrance pupil. In other words, the size to separation ratio of the reduced afocal beams entering the beam combining telescope must precisely match that of the subapertures in the entrance pupil plane.

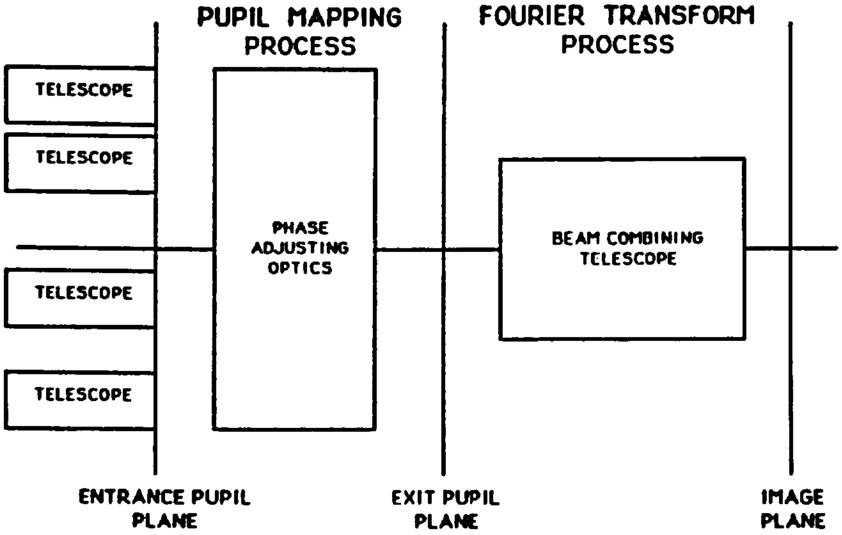

Figure 4-2. Functional diagram illustrating that imaging with a phased telescope array is a two-step process.

The phase delay Δ associated with a given subaperture due to an off-axis source at a semi-field angle θ_o is given by

$$\Delta = y_n \sin \theta_o \tag{4-1}$$

This phase delay propagates through the telescope unchanged; however, the plane wave segment emerging from the telescope has undergone an angular (tilt) magnification that is the reciprocal of the telescope transverse magnification

$$m_t = D_n'/D_n < 1 \tag{4-2}$$

It is clear from Figure 4-3 that the plane wave segments emerging from the telescopes do not lie in a plane, but in a venetian blind configuration. The beam-combining optics consist of a series of flat folding mirrors that allow for phase adjustments to be made and to reduce the coordinates of of the reduced beams so they can be collected by the single beam-combining telescope which produces the final image. The magnification of the beam-combining optics is defined as the ratio of the reduced coordinate of the nth beam to the coordinate of the nth subaperture

$$m_c = y_n'/y_n \tag{4-3}$$

Since the phase adjusters can only correct the phase errors for a single field

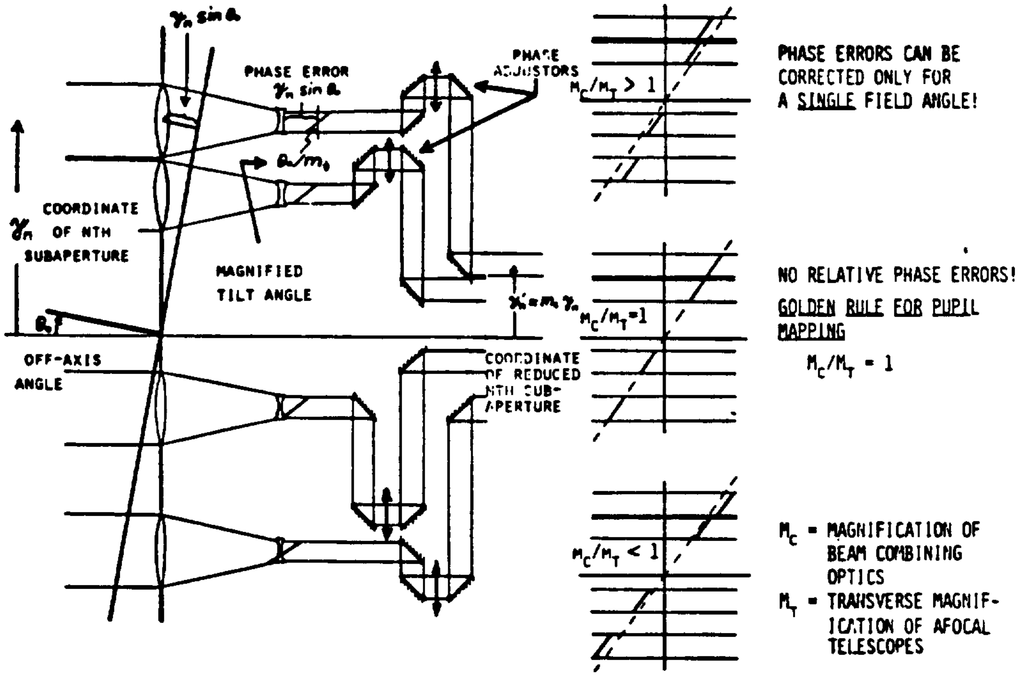

Figure 4-3. Illustration of relative phase errors when pupil mapping is not performed properly.

angle, we obtain the following requirement for imaging an extended field of view for all n telescopes

$$m_c / m_t = 1 \qquad (4\text{-}4)$$

This requirement is the Golden Rule for Pupil Mapping referred to by Traub.[3]

Reference 5 describes in detail the quantitative calculation of the image degradation due to lateral pupil mapping errors for a variety of subaperture configurations. That reference is attached as Appendix B and only the results of those calculations are presented here.

Figure 4-4 shows the image degradation, in terms of Strehl ratio, as a function of field angle for the MMT, Golay-6, and Mill's Cross configuration when there exists a pupil mapping error of 1 part in 10^4 ($m_c / m_t = 0.9999$). A subaperture diameter of 2.0 meters and a wavelength of 0.5 μm was assumed. A useful field of less than an arc minute is implied with the more dilute subaperture configurations suffering the greatest degradation.

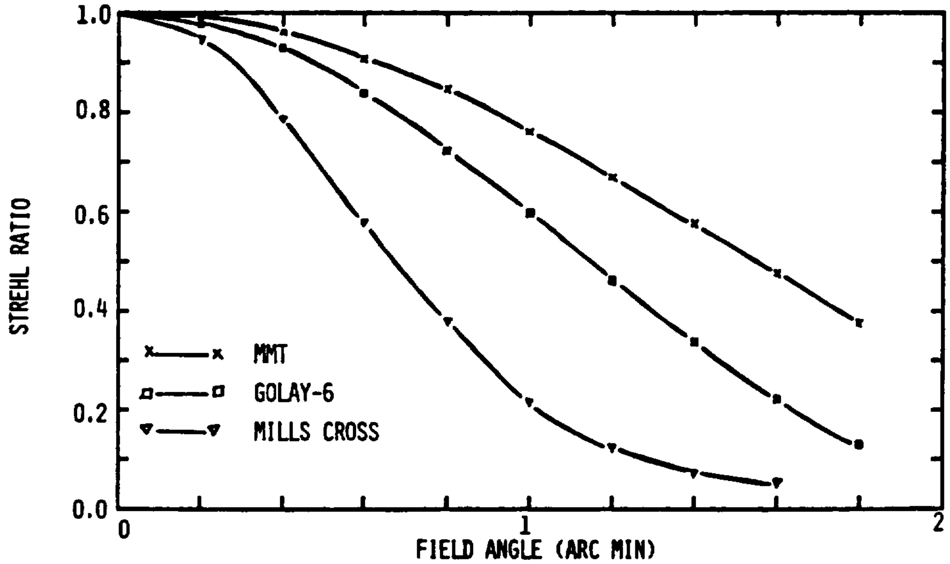

Figure 4-4. Image degradation due to a pupil mapping error of 1 part in 10^4.

The sensitivity of the image degradation due to pupil mapping errors to the telescope magnification is illustrated in Figure 4-5. For the MMT configuration and $m_c / m_t = 0.9999$ we have plotted Strehl ratio vs. field angle for m_t = 1, 1/4th, 1/10th, and 1/20th. These curves indicate that image degradation due to pupil mapping errors are not a particularly strong function of telescope magnification.

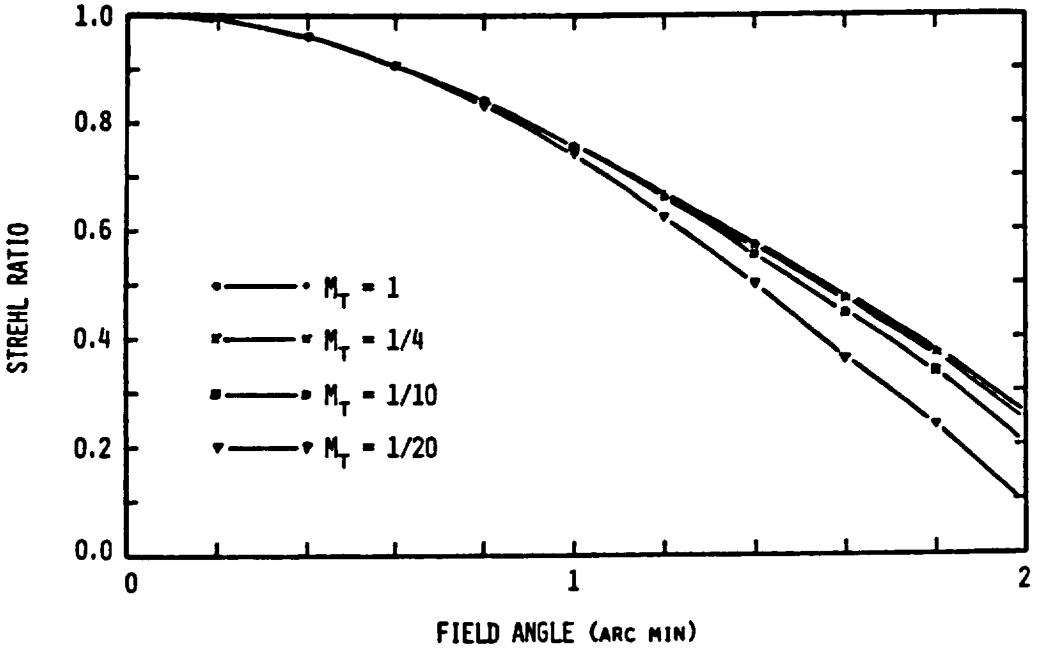

Figure 4-5. Sensitivity of image degradation to telescope magnification.

Figure 4-6 shows the sensitivity of the useful field-of-view to the magnitude of the pupil mapping error. We have arbitrarily chosen a Strehl ratio of 0.80 to define the useful field-of-view. Again we are considering a subaperture diameter diameter of 2.0 meters and a wavelength of 0.5 μm. This figure indicates that a pupil mapping error of 1 part in 10^4 will limit the field-of-view to a few tens of arc seconds, and a pupil mapping error of 1 part in 100 will permit only a sub arc second field of view.

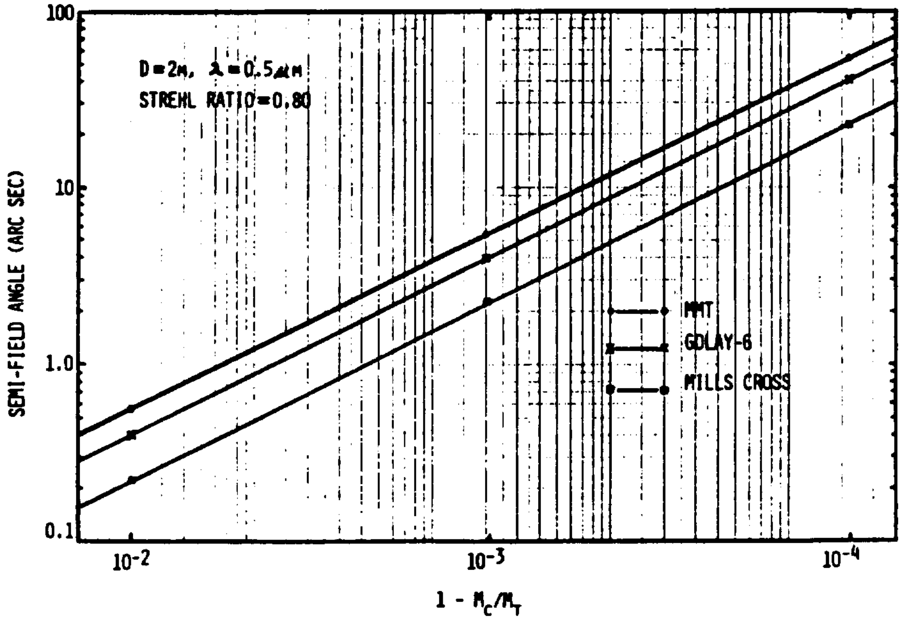

Figure 4-6. Field-of-view limitations due to pupil mapping errors.

It should be emphasized that these pupil mapping errors are not a fundamental limitation to imaging phased telescope arrays. It is an operational error determined by the ability to accurately position the folding mirrors in the beam combining optics and to maintain that position throughout the observation time in the presence of realistic environmental errors. Just as the telescope array can be phased by closing a control loop through a wavefront sensor with appropriate algorithms and driving the phase adjusting mirrors to maximize the image quality, these lateral pupil mapping errors can also be actively controlled by closing a control loop around an off-axis wavefront sensor and driving the final folding mirrors in the beam combining optics to the positions that maximize the image quality.[20,21]

4.3 AXIAL PUPIL MAPPING ERRORS AND MAGNIFICATION ERRORS

Axial (or longitudinal) pupil mapping errors result when the entrance pupils of the individual identical telescopes are not positioned precisely coplanar, or if the secondary mirrors or other optical elements following the entrance pupils of the individual telescopes are not identical. These axial pupil mapping errors are examined in detail by Weaver *et al.* in Reference 8 which attached to the report as Appendix C. He states that this error is a result of the assembly process and can never be perfect; however, they produce only a second-order effect upon image quality which can be important but does not impose positioning requirements beyond the current state of the art.

Weaver *et al.* also discusses in some detail the relative magnification errors between the various telescopes making up the phased array and their effect upon image quality. The requirement upon magnification matching is very stringent and clearly beyond the state of the art in optical fabrication of large telescopes. However, a weak zoom system can be incorporated into the telescope design that permits the magnification of each independent telescope to be adjusted until the required tolerance is achieved.

4.4 ABERRATIONS OF THE INDIVIDUAL TELESCOPES

The wavefront aberration function for a rotationally symmetric optical system can be written as

$$\begin{aligned} W = {} & W_{020}\, a^2 + W_{111}\, \beta\, a \cos\psi + W_{040}\, a^4 + W_{131}\, \beta\, a^3 \cos\psi \\ & + W_{222}\, \beta^2 a^2 \cos^2\psi + W_{220}\, \beta^2 a^2 + W_{311}\, \beta^3 a \cos\psi \qquad (4\text{-}5) \\ & + \text{ Higher Order Terms} \end{aligned}$$

where β is the normalized field parameter, a is the normalized pupil radius, and ψ is the azimuthal pupil parameter.[22]

If a two-mirror afocal telescope is properly fabricated, assembled, and pointed there will be no defocus or tilt errors. In addition, the Mersenne two-mirror afocal telescope design (confocal parabolas) exhibits no third-order spherical aberration, third-order coma, or third-order astigmatism. However, any two-mirror telescope of non-unit magnification will exhibit field curvature. Hence, only field curvature and distortion exist through third order for Mersenne telescopes. Since field curvature varies as β^2 and distortion varies as β^3, Harvey assumed that field curvature dominates distortion for small angles and proceeded to investigate the effects of field curvature of the individual telescopes upon the performance of phased telescope arrays.[5]

In conventional telescopes, field curvature is a rather benign aberration since it only displaces the image of a point source axially by an amount proportional to the square of the field angle rather than smearing it as does spherical aberration, coma, or astigmatism. Therefore, by utilizing a curved focal surface no image degradation is produced.

However, in a phased telescope array, the field curvature of the individual telescopes results in a relative phase (piston) and tilt (pointing) error between the various subapertures. These two effects can rapidly degrade image quality for increasing field angles thus severely limiting the useful field-of-view of the phased telescope array.

The results of preliminary calculations performed in Reference 5 indicate that for visible light and 2.0 meter diameter individual Mersenne telescopes operated as a phased array, useful fields-of-view may be limited to a few tens of arc seconds for some subaperture configurations of interest.

This apparent fundamental field-of-view limitation of phased telescope arrays provided the impetus for the current parametric study.

5.0 DEVELOPMENT OF ERROR BUDGET TREE

5.1 REQUIREMENTS

The detailed design of a large space-based phased telescope array will depend critically upon the ability to make realistic performance predictions in the presence of error sources and to determine the tolerances necessary to meet given system performance requirements. The primary requirement for the purposes of this study is to obtain near diffraction-limited behavior (Strehl ratio > 0.8) over fields of view up to 0.5 degrees.

It has been emphasized by AFWL that they do not want us to merely evaluate a point design; hence, the technical approach is to perform parametric analyses and trade studies of the dominant error sources for a variety of telescope and subaperture configurations to determine their field-of-view limitations, then proceed to the next design in a hierarchy of telescope configurations with increasing degrees of freedom until the desired field-of-view is obtained in the telescope sizes of interest.

A systems engineering approach utilizing error budgeting techniques has been used to determine allowable error budget allocations not only for residual design aberrations but for state-of-the-art optical fabrication and alignment errors as well. In this manner one can derive the realistic design and engineering tolerances and their scaling behavior for imaging phased telescope arrays.

5.2 PRELIMINARY ERROR BUDGET TREE

A comprehensive list of potential error sources that might degrade the optical performance of imaging phased telescope arrays was first tabulated. These error sources were then categorized and put into the form of a error budget tree as illustrated in Figure 5-1. Note that we have chosen four primary categories that will follow the chronological development of a phased telescope array program from design, through fabrication, assembly and alignment, to launch and operation in the space environment.

The top level requirement was taken to be an off-axis image quality degradation at the edge of the field of view no greater than that represented by a Strehl ratio of 0.80. A preliminary tops-down error budget allocation (Strehl ratio > 0.946) was then assigned to each of the error source categories. These allocations were then further broken down among the error sources in each category. This is merely the starting point for a bottoms-up error budgeting process involving reallocation by applying engineering experience and detailed analysis of the individual error sources in an attempt to achieve an equitable distribution difficulty.

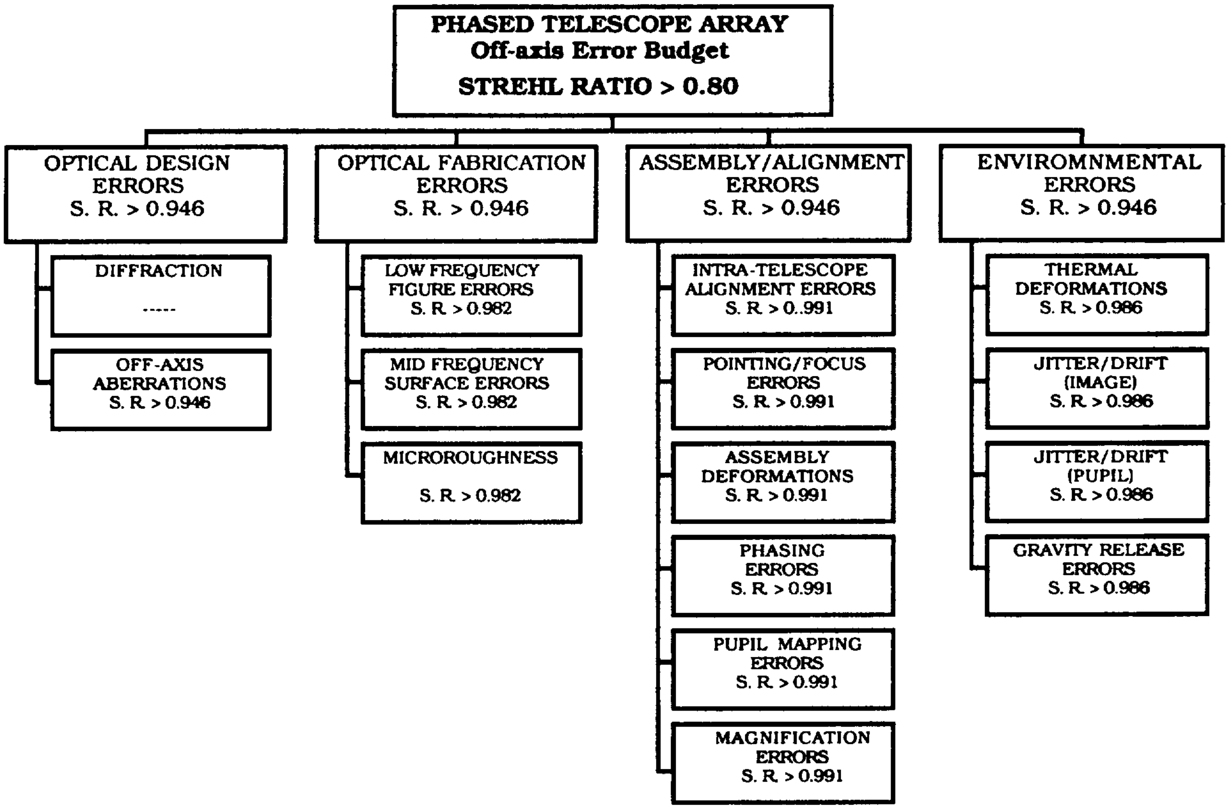

Figure 5-1. Error budget tree form with preliminary tops-down allocations expressed in terms of degradation of the Strehl ratio.

The next step in the development of an error budget tree for imaging phased telescope arrays was to convert the allocations expressed in terms of Strehl ratio to allocations expressed in terms of the more conventional rms wavefront error. Using the following expression for Strehl ratio,[23]

$$\text{Strehl ratio} = \exp[-(2\pi\sigma_W/\lambda)^2] \qquad (5\text{-}1)$$

the top level off-axis optical performance requirement corresponds to an rms wavefront error of less than 0.075 waves at the operational wavelength. Figure 5-2 is the same error budget as that presented in Figure 5-1 with all of the allocations converted to rms wavefront error.

Some of these preliminary allocations are probably easy to achieve while others may be impossible to achieve. The next task is to perform a detailed bottoms-up reallocation of each error source in an attempt to equalize the difficulty of achieving the performance required by each allocation. This is the optimum condition that will reduce risk and development costs for the program.

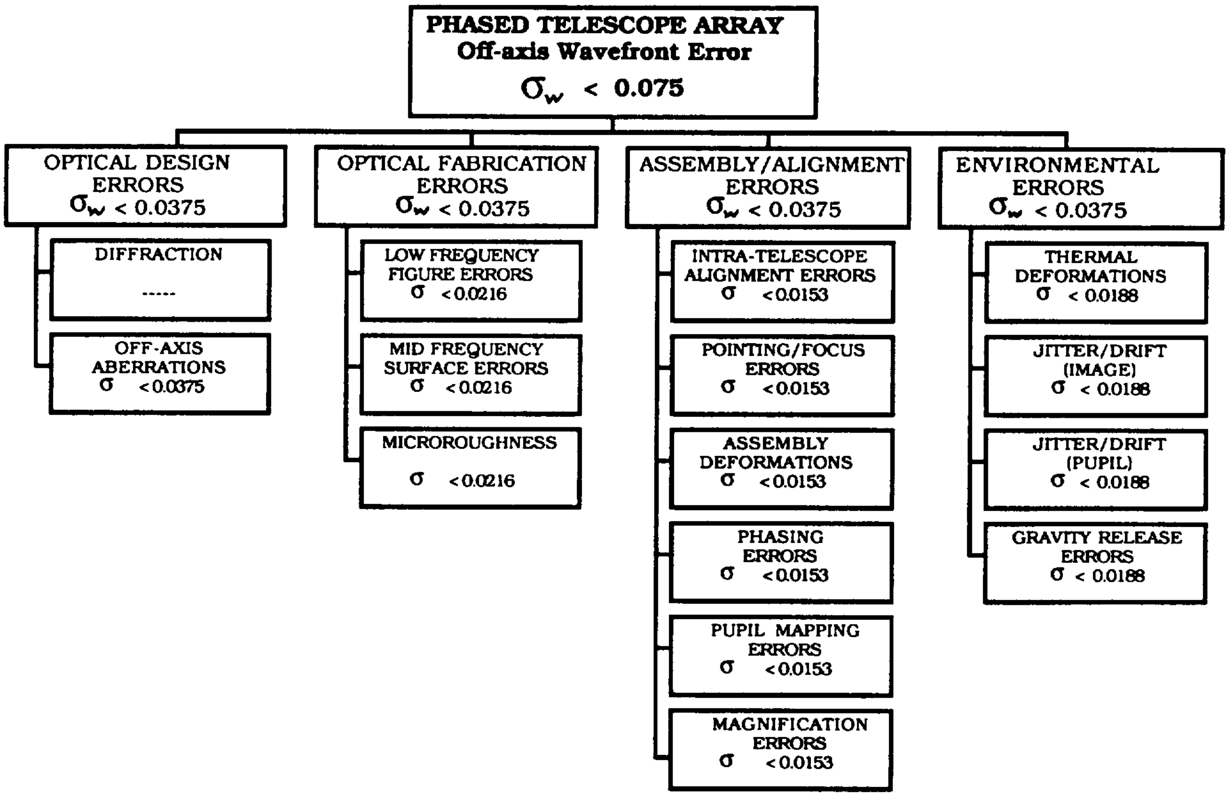

Figure 5-2. Error budget tree with preliminary tops-down allocations converted to rms wavefront error.

5.2.1 Off-axis Error Budget

Perkin-Elmer's state-of-the-art experience with the optical fabrication of large precision optics was then applied to the reallocation of the optical fabrication errors. The Hubble Space Telescope (HST) error budget allowed an rms wavefront error of 0.04 waves ($\lambda = 0.6328$ μm) for optical fabrication errors for the primary and secondary mirror combined.[24] The Solar Optical Telescope (SOT) error budget allows a slightly increased rms wavefront error of $\sigma_w < 0.05$ waves but includes a tertiary mirror.[25] We thus chose the smaller allocation of $\sigma_w < 0.04$ waves as a realistic state-of-the-art allocation for optical fabrication errors for a phased telescope array. The relative fraction of this allocation given to low spatial frequency figure errors and mid spatial frequency surface errors was taken from the SOT error budget. The microroughness would undoubtably be given a specification based upon separate scattering requirements.

The intra-telescope alignment errors and assembly deformations were similarly taken from Perkin-Elmer's engineering experience on such programs as the HST and the SOT. The allocation of $\sigma_w < 0.0250$ waves for phasing errors is based upon the successful laboratory demonstration of the PHASAR Telescope being phased to approximately $\lambda/15$ and the assumption that this performance can be improved upon in the future.[20]

The error budget allocation of $\sigma_W < 0.0150$ waves for relative pointing and focus errors was also chosen to be consistent with previously referenced studies and experiments.[8,14,20]

The final two error sources in the assembly and alignment category are the pupil mapping errors and relative magnification errors previously discussed as being particularly important in wide field-of-view imaging applications utilizing phased telescope arrays. These are not fundamental problems as are the residual optical design aberrations; however, they pose severe engineering challenges in the positioning and operation of these complex optical systems. Rms wavefront error allocations of $\sigma_W < 0.0150$ waves were given to these two error sources.

When these error budget allocations are root-sum-squared (rss'd), they result in a total allocation of $\sigma_W < 0.0404$ for assembly and alignment errors as illustrated in Figure 5-3.

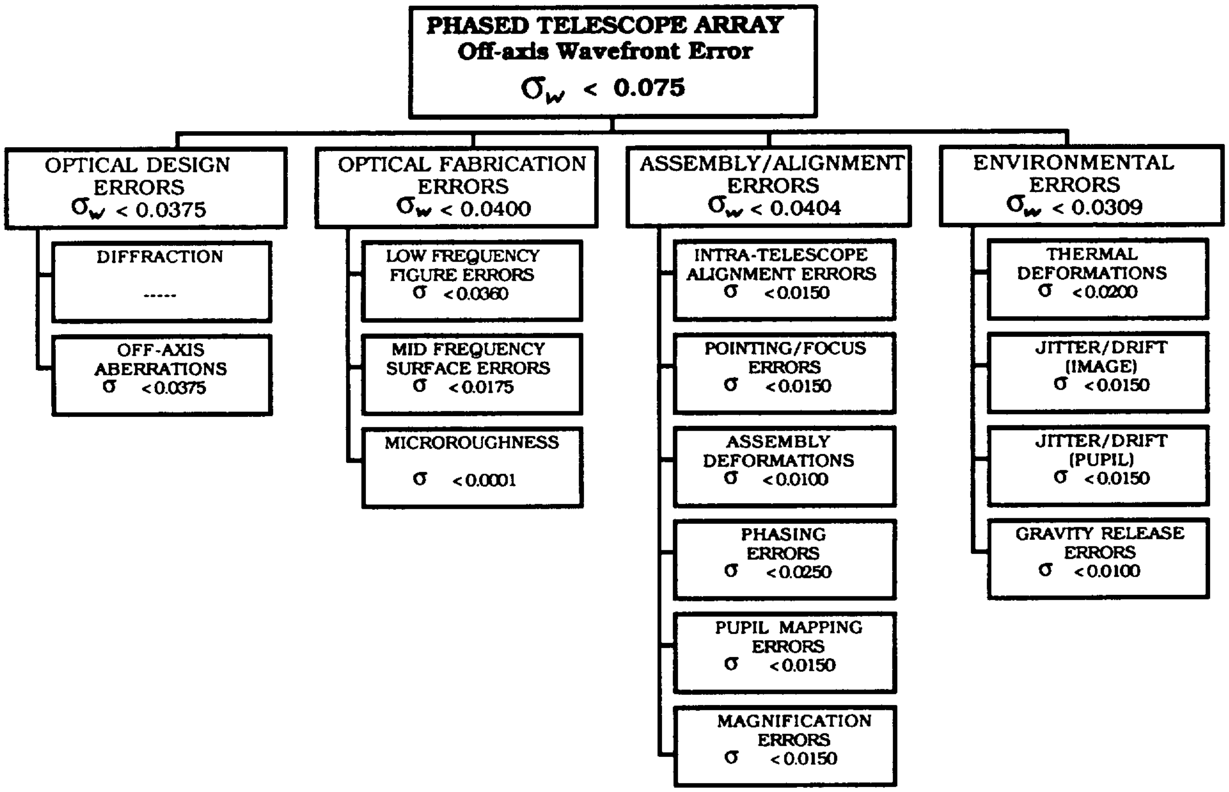

Figure 5-3. Off-axis Error Budget Resulting from Bottoms-up Reallocation of Individual Error Sources.

Finally, the allowable contributions from error sources in the category of environmental errors were adjusted from their preliminary values. The allocation of $\sigma_W < 0.0200$ for thermal deformations is again consistent with error budget allocations on the HST. In addition to the usual allocation for image jitter and drift, for phased telescope arrays we must also put a limit upon pupil jitter and drift (dynamic pupil mapping errors). An rms wavefront error of $\sigma_w < 0.0150$ was thus estimated for these two error sources. A preliminary allocation of $\sigma_w < 0.0100$ for gravity release errors due to built-in stresses caused by assembly and alignment of the individual telescopes in a 1 g gravitational field is provided (an estimate to be verified by further analysis). These allocations rss up to a value of $\sigma_w < 0.0309$ for all environmental errors.

5.2.2 On-axis Error Budget for Phased Array

Some of the error sources included in the previous off-axis error budgets affect only the off-axis optical performance while others degrade the on-axis image quality as well. In Figure 5-4 we have shaded those error sources which affect only the off-axis optical performance (without changing any of the individual error source allocations) and have eliminated their contributions to the top-level rms wavefront error. These include the off-axis aberrations under optical design errors, the pupil mapping errors and relative magnification errors under assembly and alignment errors, and the pupil jitter and drift under environmental errors. The resulting top-level on-axis optical performance prediction is an rms wavefront error of $\sigma_w < 0.0600$ which corresponds to a Strehl ratio of 0.8675.

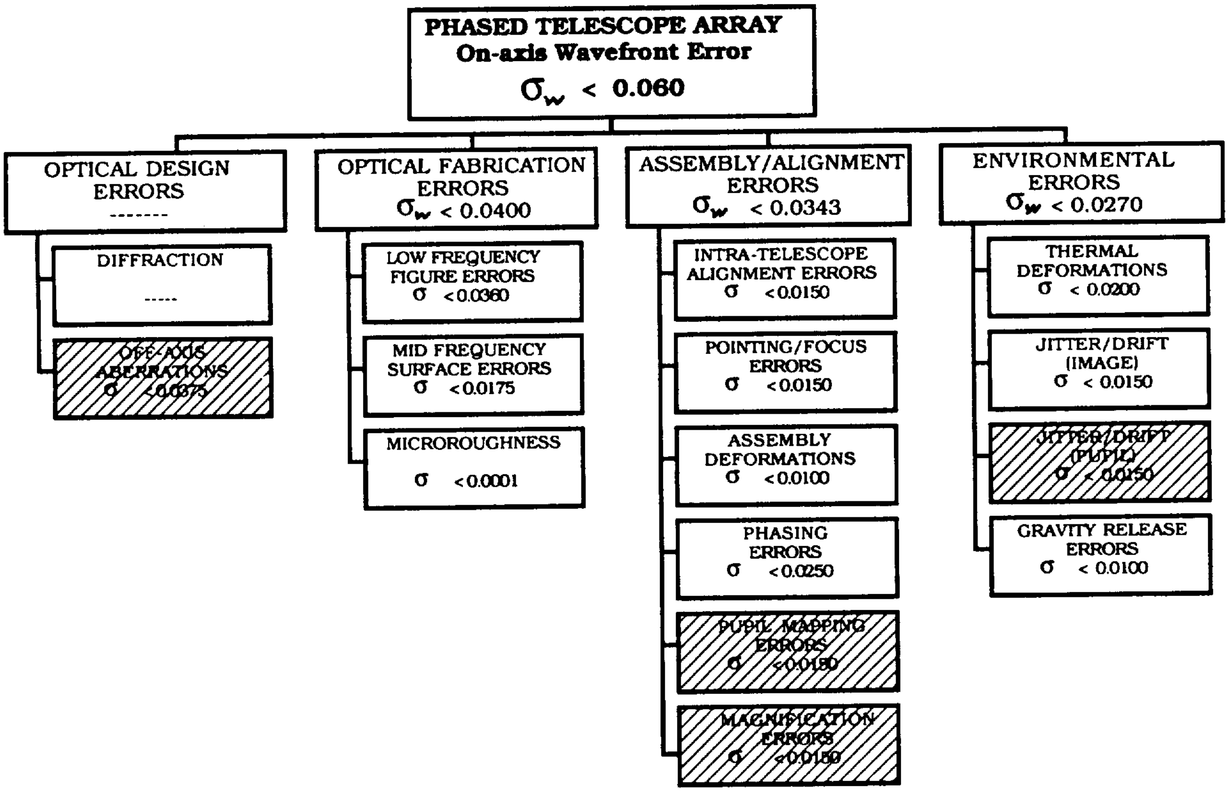

Figure 5-4. On-axis performance prediction resulting from reallocation of individual on-axis error sources.

This top-level on-axis requirement of a residual rms wavefront error of $\sigma_W < 0.0600$ is the same as that specified for the SOT program and slightly relaxed from that specified for the HST program ($\sigma_W < 0.0500$). However, those two telescopes, while state-of-the-art, do not have any of the error sources unique to phased telescope arrays; in particular, the relative pointing and focusing errors, the phasing errors, and most of the image jitter and drift allocation.

5.2.2 On-axis Error Budget for Independent Telescope

In Figure 5-5 we have therefore shaded (different cross-hatch) those additional error sources and eliminated their allocations to obtain an error budget tree for a single independent telescope making up the array. The top-level on-axis requirement ($\sigma_W < 0.0493$) for each independent telescope is now slightly tighter than that for the Hubble Space Telescope.

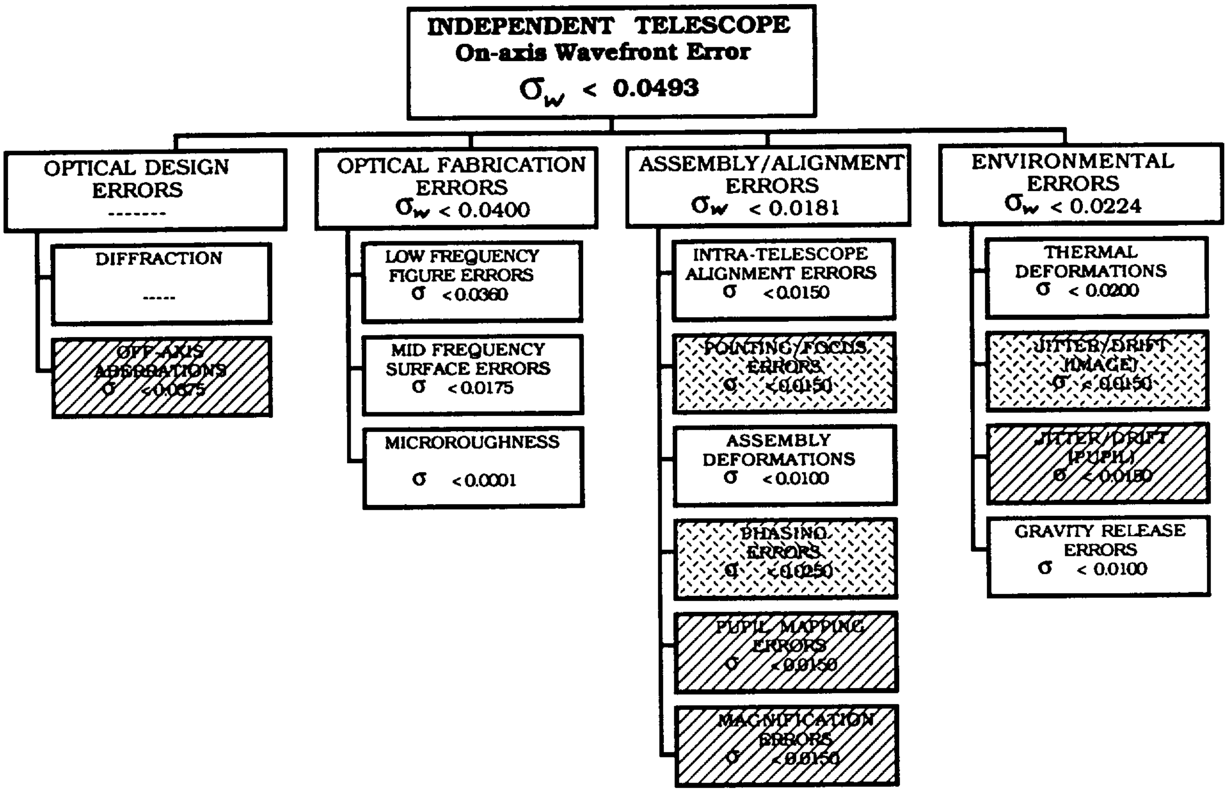

Figure 5-5. On-axis Error Budget for a single telescope making up the array (exhibiting the same top-level requirement as HST).

This, coincidentally, leaves the original allocation of $\sigma_w < 0.0375$ (or degradation of the Strehl ratio to a value of 0.95) for the optical design errors due to off-axis aberrations of the individual telescopes. And it is the effects of these aberrations that will be studied parametrically in the following sections of this report to determine whether wide fields can be achieved (as constrained by this error budget allocation) as the phased telescope arrays are scaled up in size.

Clearly these error budget allocations will be adjusted in the future as technological developments are made or additional knowledge is acquired concerning these very complex optical systems.

6.0 PARAMETRIC STUDIES, SENSITIVITY ANALYSES, AND SCALING BEHAVIOR

The absence of a purturbing atmosphere in space-based applications permits the possibility of achieving high resolution over a substantial field-of-view with phased telescope arrays if the error sources discussed in the previous section of this report are adequately controlled. Many of these error sources have been discussed in the literature as evidenced by our fairly extensive list of references. Ironically, the most frequently ignored potential error source is also perhaps the most basic and fundamental, i.e., the inherent aberrations of the optical design chosen for the individual telescopes. It is the field-of-view limitations of these residual optical design errors (off-axis aberrations) that is going to be emphasized in the remainder of this report.

6.1 DIFFRACTION-LIMITED PERFORMANCE

The diffraction-limited performance of an optical system should be understood before discussing the degradation of that diffraction-limited performance by aberrations. As stated in Section 3 of this report the Strehl ratio has been chosen as the image quality criterion for this study. The Strehl ratio is defined as the peak irradiance of an aberrated point spread function (PSF) divided by the peak irradiance of the diffraction-limited PSF for a given optical system. The diffraction-limited PSF of a synthetic aperture array made up of circular subapertures of diameter D is given by

$$I(x,y) = (\pi D^2/4\lambda f)^2 \, [2 \, J_1(\pi r D/\lambda f)/(\pi r D/\lambda f)]$$

$$\times \; \left| \sum_{n=1}^{N} \exp[i2\pi(x \, x_n + y \, y_n)/\lambda f] \right|^2 \tag{6-1}$$

Note that this is merely an interference term multiplied by an envelope function given by the irradiance distribution that would be produced by a single circular subaperture.

Harvey has calculated and compared the PSF profiles and fractional encircled energy curves for a variety of both dilute and close-packed circular subaperture configurations.[5,26]

6-2 EFFECTS OF TELESCOPE ABERRATIONS

As previously stated in Section 4, the wavefront aberration function for a rotationally symmetric optical system can be written as

$$W = W_{020}\ a^2 + W_{111}\ \beta\, a \cos\psi + W_{040}\, a^4 + W_{131}\ \beta\, a^3 \cos\psi$$

$$+ W_{222}\ \beta^2 a^2 \cos^2\psi\ +\ W_{220}\ \beta^2 a^2\ +\ W_{311}\ \beta^3 a \cos\psi \qquad (6\text{-}2)$$

$$+\ \text{Higher Order Terms}$$

where β is the normalized field parameter, a is the normalized pupil radius, and ψ is the azimuthal pupil parameter.[22] The first two terms in this aberration expansion are the 1st-order aberrations commonly referred to as defocus and tilt (or lateral magnification error). The next five terms are the 3rd-order (Seidel) aberrations which have traditionally been called spherical aberration, coma, astigmatism, field curvature, and distortion.

We will start our parametric study with an array of two-mirror afocal telescopes of the Mersenne design (confocal paraboloids) as previously shown in Figure 3-5. If properly fabricated, assembled, and pointed there will be no defocus or tilt errors. Furthermore, this particular telescope design, illustrated schematically in Figure 6-1, is also inherently free of third-order spherical aberration, coma, and astigmatism. However, any two-mirror telescope of non-unit magnification will exhibit field curvature. Hence, only field curvature and distortion exist through third order for Mersenne telescopes.

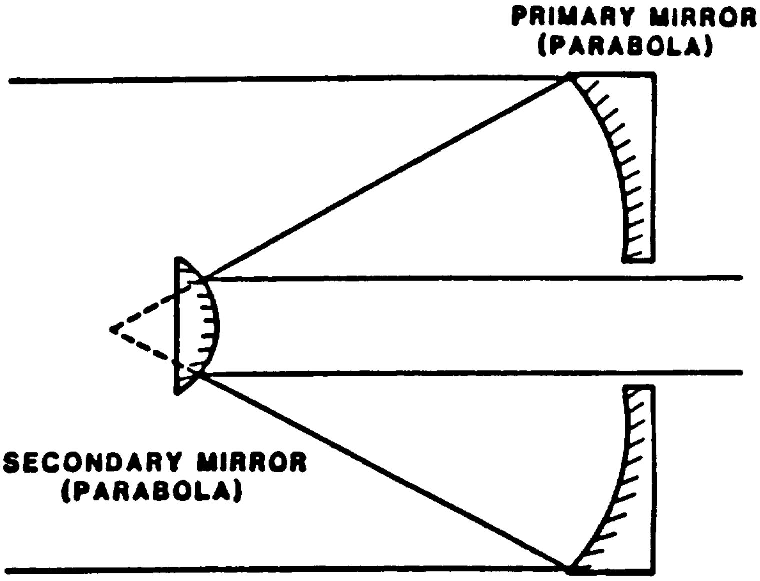

Figure 6-1. Mersenne afocal telescope designs consisting of two confocal paraboloids have no third-order spherical aberration, coma, or astigmatism but do exhibit field curvature and distortion.

The magnitude of the field curvature coefficient is determined by the primary mirror diameter (D_p), its F/no. (F_p), the telescope magnification (m), and the field angle (θ_o). For Mersenne telescopes[27]

$$\text{Field Curvature} = W_{20} = [\, D_p / (16\, F_p)]\, [(1 - m)/m]\, \theta_o^2 \qquad (6\text{-}3)$$

Similarly, the magnitude of the distortion coefficient is given by [27]

$$\text{Distortion} = W_{11} = (D_p / 8)\, [(3m + 1)(m - 1)/m^2]\, \theta_o^3 \qquad (6\text{-}4)$$

Since field curvature varies as θ_o^2 and distortion varies as θ_o^3, it is clear that field curvature will dominate distortion for small field angles and distortion will dominate field curvature at sufficiently large field angles. Figure 6-2 shows quantitatively that this cross-over point occurs at a field angle of about one degree for a 2 meter diameter telescope with a F/2.5 primary mirror and a magnification of 0.1. Furthermore for field angles less than five arc minutes, the field curvature coefficient is at least an order of magnitude larger than distortion. We will thus concern ourselves only with field curvature in the preliminary analysis of phased arrays of two-mirror telescopes.

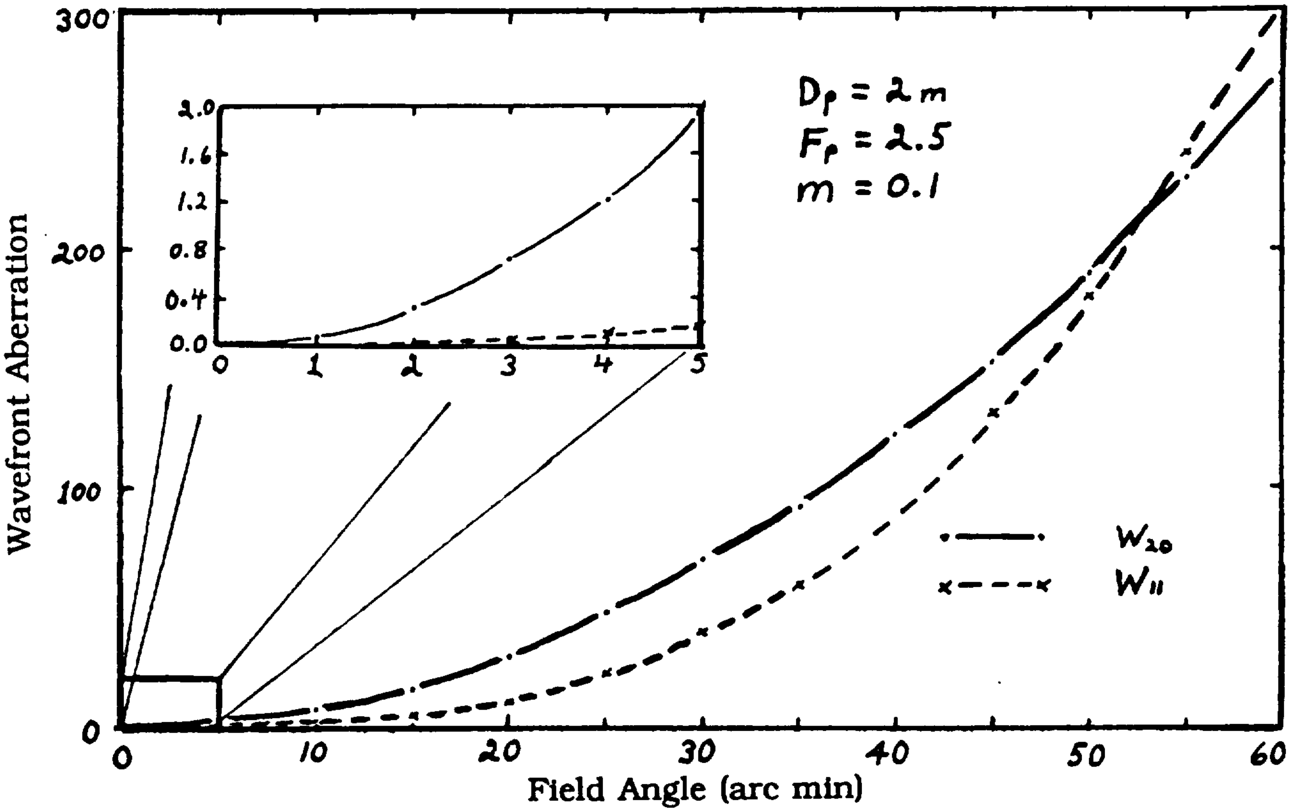

Figure 6-2. Field curvature dominates distortion at small field angles.

In conventional telescopes, field curvature is a rather benign aberration since it only displaces the image of a point source axially by an amount proportional to the square of the field angle rather than smearing it as does spherical aberration, coma, or astigmatism. Therefore, by utilizing a curved focal surface no image degradation is produced.

However, in a phased telescope array, the field curvature of the individual telescopes results in a wavefront error over the nth subaperture given by

$$W_n(x, y) = W_{20}\, r^2 = W_{20}\,(x^2 + y^2) \qquad (6\text{-}5)$$

When referenced to the array coordinate system

$$W_n(x', y') = W_{20}\,[(x' - x_n)^2 + (y' - y_n)^2] \qquad (6\text{-}6)$$

where x_n and y_n are the coordinates of the nth subaperture as shown in Figure 6-3.

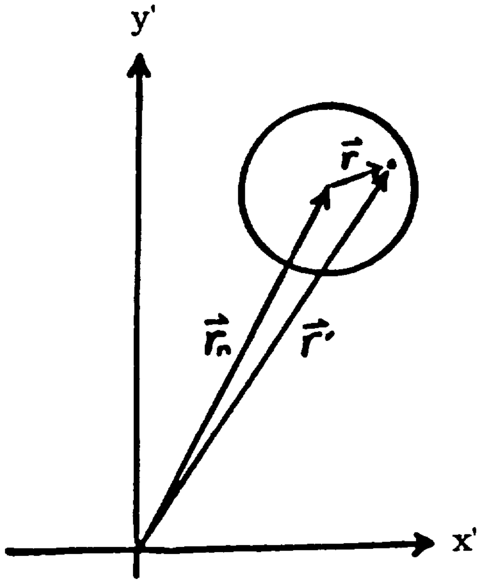

Figure 6-3. Relationship between subaperture and array coordinates.

Eq. (6-6) can be rewritten as

$$W_n = W_{20}\, r_n^2 - 2\, W_{20}\,(x'\, x_n + y'\, y_n) + W_{20}\, r'^2 \qquad (6\text{-}7)$$

The first term is a relative phase (piston) error between the various subapertures and the second term is a relative wavefront tilt (or pointing error) between the subapertures. These two terms can rapidly degrade image quality for increasing field angles thus severely limiting the useful field of view of the phased telescope array. The third term is a conventional field curvature for the array which can be partially compensated by utilizing a curved focal surface for the beam combining telescope.

It should be noted that the first two terms of Eq. (6-7) depend upon the position coordinates of the subapertures; hence, the achievable field-of-view may vary substantially with subaperture configuration. Also, the first term can be cancelled by repositioning the phase adjusting mirrors; however, this can be done for only one field position. Hence, this does not increase the field-of-view, but it does provide a convenient mechanism for agile pointing of the phased telescope array over a limited angular range without slewing the array (or even the individual telescopes).

6.3 COMPUTATIONAL TECHNIQUES

Three different techniques of calculating the image degradation of phased telescope arrays due to the aberrations of the individual telescopes were employed in this study: 1.) an analytical expression for the Strehl ratio was derived for some situations; 2.) an analytical expression for the rms wavefront error, σ_w, was derived for the case where field curvature is the dominant aberration present; and 3.) a computer code was developed to numerically calculate the rms wavefront error in the presence of arbitrary aberrations. Each of these techniques will be discussed in some detail.

6.3.1 Analytical Solution for Strehl Ratio

This first method of calculating the Strehl ratio of phased telescope arrays was used in Reference 5 in an attempt to describe the effects of field curvature of the individual telescopes. Overly pessimistic results were obtained because we completely discarded the last term of Eq. (6-7), arguing that this term could be compensated for by invoking a curved focal surface for the beam combining telescope. This resulted in the following analytical solution for the Strehl ratio

$$\text{Strehl ratio} = (1/N^2)\left|\sum_{n=1}^{N} \text{somb}(2\,\hat{W}_{20}\,\hat{r}_n\,\hat{D})\,\exp(-i2\pi\,\hat{W}_{20}\,\hat{r}_n^2)\right|^2 \qquad (6\text{-}8)$$

where

$$\text{somb}(r/d) = 2\,J_1(\pi\,r/d)/(\pi\,r/d) \qquad (6\text{-}9)$$

as defined by Gaskill,[28] and $\hat{W}_{20} = W_{20}/\lambda$, $\hat{r}_n = r_n/\lambda$, $\hat{D} = D/\lambda$, etc.

Figure 6-4 graphically illustrates the Strehl ratio vs. field angle for several different subaperture configurations when we fix the various parameters as indicated. Figure 6-5 is a similar graph of Strehl ratio vs. field angle for several different Circle-N configurations. Note that all of the Circle-N configurations perform better than any of the configurations with radial variations in the position of the subapertures.

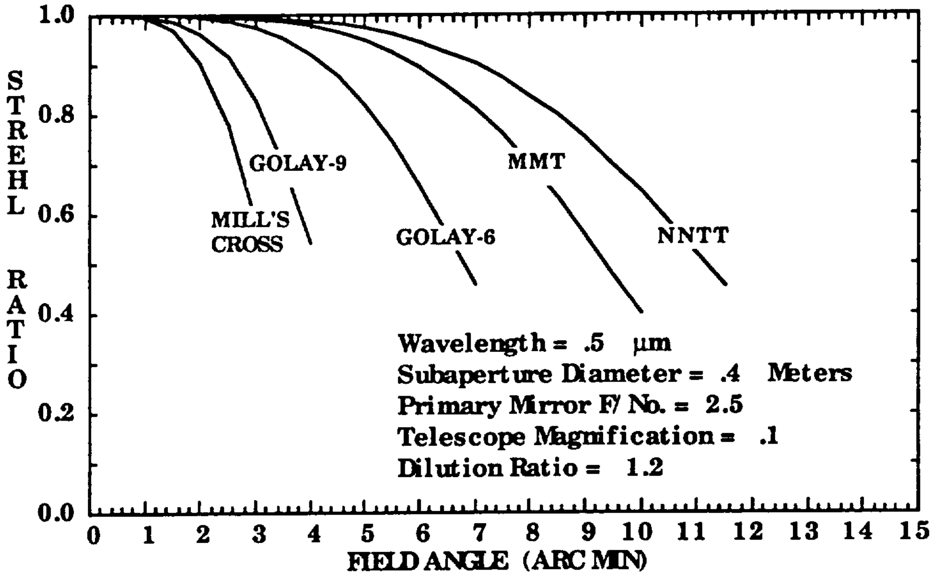

Figure 6-4. Strehl ratio vs. field angle for various subaperture configurations when all subapertures are the same size .

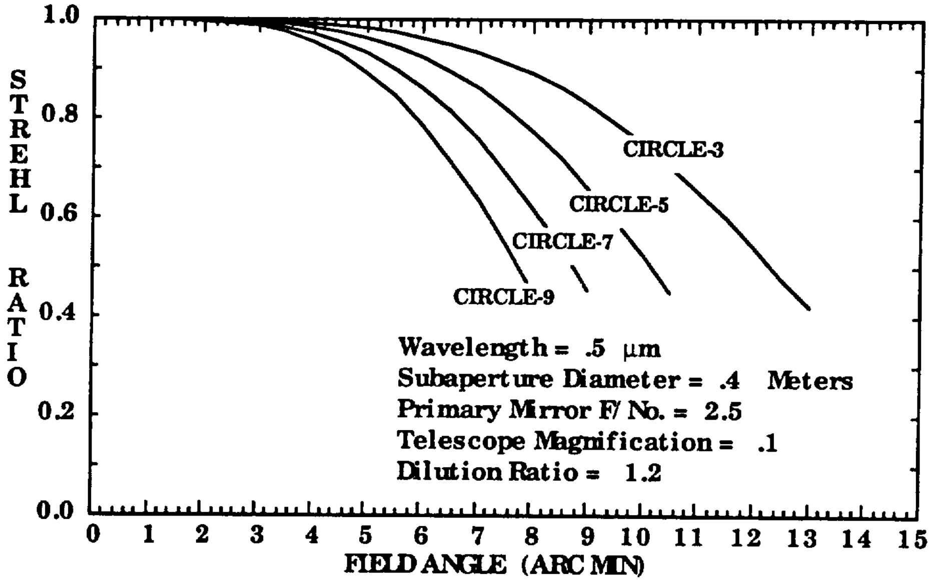

Figure 6-5. Strehl ratio vs. field angle for Circle-N subaperture configurations when all subapertures are the same size.

If we hold the total collecting area constant (Area = $\pi D^2/4$), i.e. let the diameter of the subapertures be equal to $D_n = D/\sqrt{N}$, then the Circle-N configurations appear to outperform the configurations with radial variations in the position of the subapertures by an even greater margin as illustrated in Figures 6-6 and 6-7.

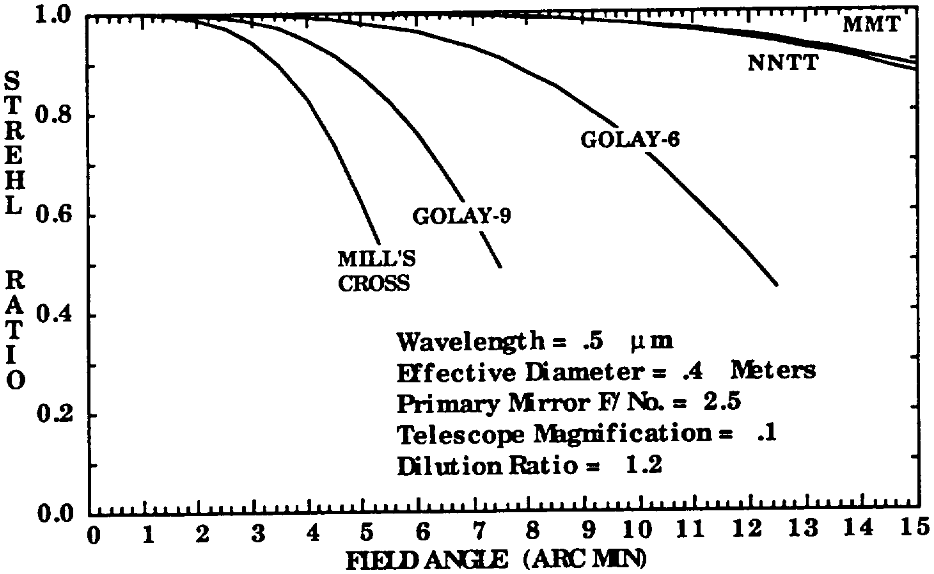

Figure 6-6. Strehl ratio vs. field angle for various configurations when the total collecting area is held constant ($D_n = D/\sqrt{N}$).

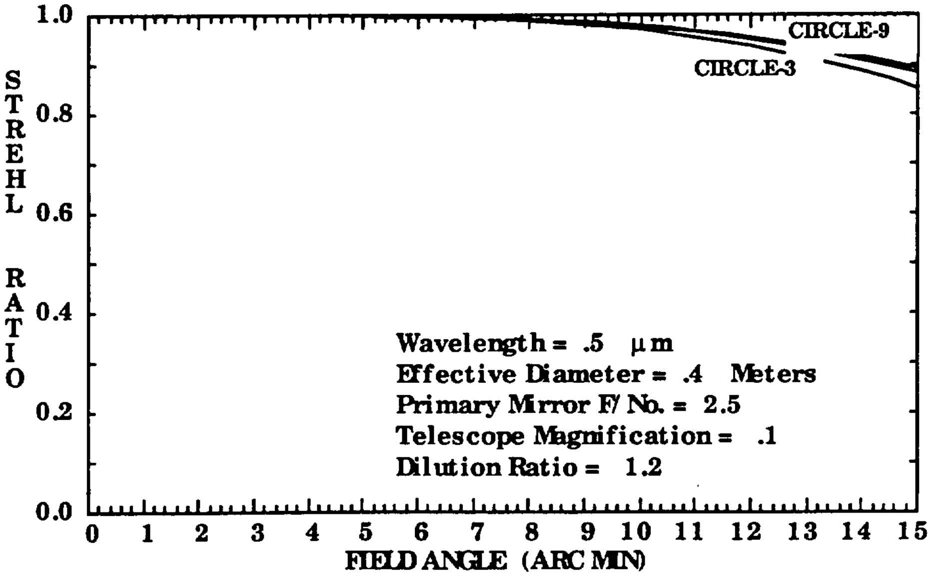

Figure 6-7. Strehl ratio vs. field angle for Circle-N configurations when the total collecting area is held constant ($D_n = D/\sqrt{N}$).

However, completely discarding the array field curvature term was equivalent to choosing a non-optimum curved focal surface for the beam combining telescope. This effect will be discussed in detail in the following section. Also some typographic errors and/or algebraic mistakes exist in Eq. (26), Eq.(27), and Eq.(29) of Reference 5. These mistakes are corrected in Appendix C of this report.

6.3.2 Analytical Solution for Wavefront Variance

Recognizing the non-optimum results predicted by the method discussed above, we proceeded to derive an analytical expression for the wavefront variance of a phased telescope array due to the field curvature of the individual telescopes. If we sum the contributions of the wavefront error described in Eq.(6-7) over the subapertures making up the array, and add an arbitrary amount of array field curvature (W_{20}') corresponding to a curved focal surface in the beam combining telescope, we obtain the following expression for the wavefront error for the entire array

$$W = \sum_{n=1}^{N} W_n \, r^2 \; C_n - \sum_{n=1}^{N} W_{20}' \, r'^2 \; C_n \qquad (6\text{-}10)$$

where

$$C_n = \mathrm{cyl}[(r' - r_n)/D] \qquad (6\text{-}11)$$

is a shifted cylinder (tophat) function of diameter D as defined by Gaskill.[28]

When we substitute Eq.(6-7) into Eq.(6-10) and rearrange, we obtain

$$W = \sum_{n=1}^{N} W_{20} \, r_n^2 \, C_n - \sum_{n=1}^{N} 2\, W_{20} \, (x_n x' + y_n y')\, C_n + \sum_{n=1}^{N} (W_{20} - W_{20}')\, r_n'^2 \, C_n \qquad (6\text{-}12)$$

Factoring out W_{20} and setting

$$q = W_{20}'/W_{20} \qquad (6\text{-}13)$$

we obtain

$$W = W_{20} \left[\sum_{n=1}^{N} r_n^2 \, C_n - 2 \sum_{n=1}^{N} (x_n x' + y_n y')\, C_n + (1 - q) \sum_{n=1}^{N} r_n'^2 \, C_n \right] \qquad (6\text{-}14)$$

We now proceed to calculate the wavefront variance

$$\sigma_w^2 = \overline{W^2} - \overline{W}^2 = (NA)^{-1} \iint_{-\infty}^{\infty} W^2 \, dx' \, dy' - \left[(NA)^{-1} \iint_{-\infty}^{\infty} W \, dx' \, dy'\right]^2 \qquad (6\text{-}15)$$

where N is the number of subapertures and

$$A = \text{area of subaperture} = \pi D^2/4 = \pi r_0^2 . \qquad (6\text{-}16)$$

Substituting Eq.(6-14) into Eq.(6-15) and performing some tedious algebra (derivation provided in detail in Appendix D) we finally obtain the following expression for the wavefront variance in terms of the subaperture configuration parameters

$$\sigma_w^2 = (W_{20}\, r_0^2)^2 \left[q^2\, r_{ms} + q^2\, \sigma_r^2 + (1 - q)^2/12 \right] \qquad (6\text{-}17)$$

where

$$r_{ms} = \overline{(r_n/r_0)^2} \qquad (6\text{-}18)$$

is the normalized mean square radius of the subaperture array, and

$$\sigma_r^2 = \overline{(r_n/r_0)^4} - \overline{(r_n/r_0)^2}^{\,2} = \overline{(r_n/r_0)^4} - r_{ms}^{\,2} \qquad (6\text{-}19)$$

is the variance in the square of the subaperture radial position about that mean square radius as illustrated in Figure 6-8.

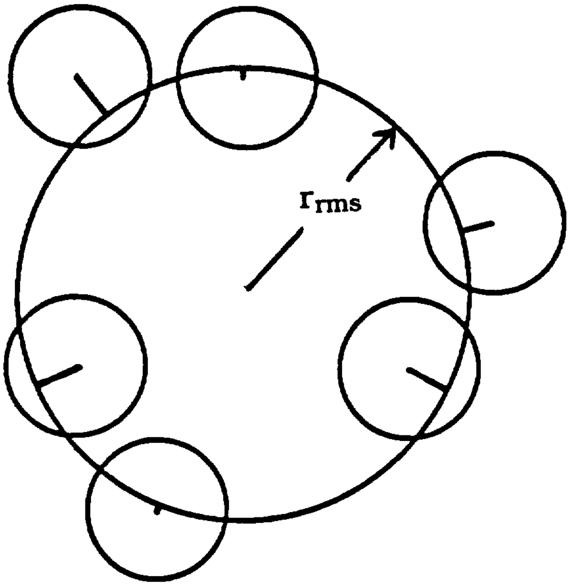

Figure 6-8. Array configuration with rms radius and the deviation of the various subapertures from that rms radius indicated.

Since σ_w^2 consists of three positive definite terms, it follows that, for any value of $q \neq 0$, σ_w^2 is a minimum when σ_r^2 is zero, i.e., when all of the subapertures are centered on a circle as illustrated in Figure 6-9.

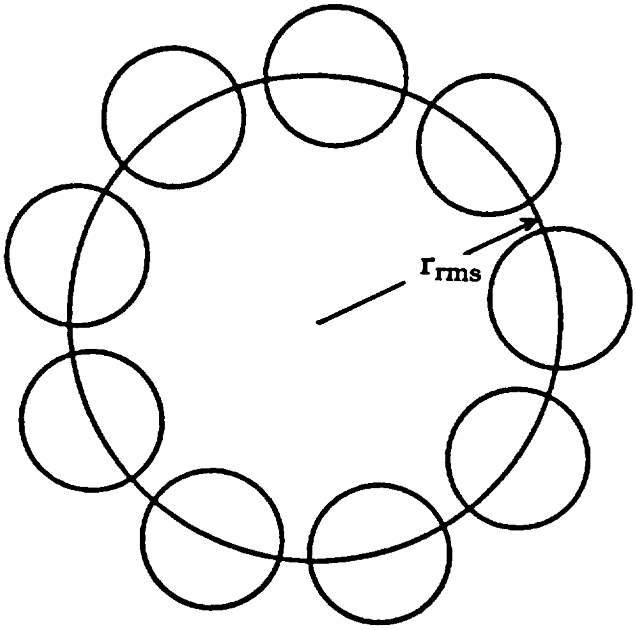

Figure 6-9. Circle-N subaperture configuration where $\sigma_r^2 = 0$.

Recall that the parameter q is the ratio of the field curvature equivalent of the curved focal surface and the field curvature of the individual telescopes. Taking the derivative of σ_r^2 with respect to the parameter q and setting the resulting quantity equal to zero, we can find an extremum for σ_r^2

$$\partial\sigma_w^2/\partial q = (W_{20}\ r_0^2\ )^2\ (\ 2\ q\ \ r_{ms}\ \ + 2\ q\ \sigma_r^2\ \ - 2\ (1 - q)/12) = 0 \qquad (6\text{-}20)$$

Since the second derivative is positive

$$\partial^2\sigma_w^2/\partial q^2 = 2(W_{20}\ r_0^2\ )^2\ [\ r_{ms}\ \ + \ \sigma_r^2\ \ + 1/12]\ > 0 \qquad (6\text{-}21)$$

that extremum is in fact a minimum. Eq.(6-20) can now be solved for the optimum value of the parameter q

$$q_{opt}\ \ = (1/12\ )/[\ r_{ms}\ \ + \sigma_r^2\ \ + 1/12] \qquad (6\text{-}22)$$

Note that q_{opt} is always less than unity. Substituting this value of q back into Eq.(6-17) provides the minimum achievable wavefront variance

$$\sigma_{wmin}^2\ = (W_{20}\ r_0^2\ )^2\ [\ q_{opt}^2\ \ r_{ms}\ \ + q_{opt}^2\ \ \sigma_r^2\ \ + (1 - q_{opt}\ )^2/12\ ] \qquad (6\text{-}23)$$

where q_{opt} corresponds to the the optimum focal surface.

This maximum performance of each subaperture configuration will thus occur at the respective values of q_{opt} as determined by Eq.(6-22). These values are tabulated below.

Table 6-1. Optimum Focal Surface for Various Subaperture Configurations

Configuration	q_{opt}
Monolith	1.0000
Circle-3	0.0416
NNTT	0.0281
MMT	0.0143
Circle-9	0.0067
Golay-6	0.0039
Golay-9	0.0005
Mill's Cross	0.0002

However, when q = 0 (the condition which corresponds to a flat focal surface), Eq(6-17) reduces to

$$\sigma_w^2 = (W_{20}\, r_0^2\,)^2/12 \tag{6-24}$$

and the wavefront variance of a phased telescope array depends only upon the field curvature of the individual subapertures and their size, and does <u>not</u> depend upon the subaperture configuration. Note that this is the well-known variance of a defocused wavefront over a single circular pupil, i.e. the wavefront variance of an aperture made up of N identical circular subapertures each with the same amount of field curvature is just the wavefront variance of one of the subapertures.

For a monolithic circular aperture (conventional telescope), $\sigma_r^2 = 0$ and $r_{ms} = 0$; hence, Eq.(6-17) reduces to

$$\sigma_w^2 = (W_{20}\, r_0^2\,)^2\,(1 - q)^2/12 \tag{6-25}$$

When q = 1, which corresponds to optimally curved focal surface for a monolith

$$\sigma_w^2 = 0 \tag{6-26}$$

Hence, there is no image degradation on this optimally curved focal surface due to field curvature for conventional monolithic imaging systems.

The image quality as a function of the parameter q is illustrated graphically in Figure 6-10 for a variety of subaperture configurations including the monolithic circular aperture. The Strehl ratio is calculated from the wavefront variance by invoking Eq.(5-1).

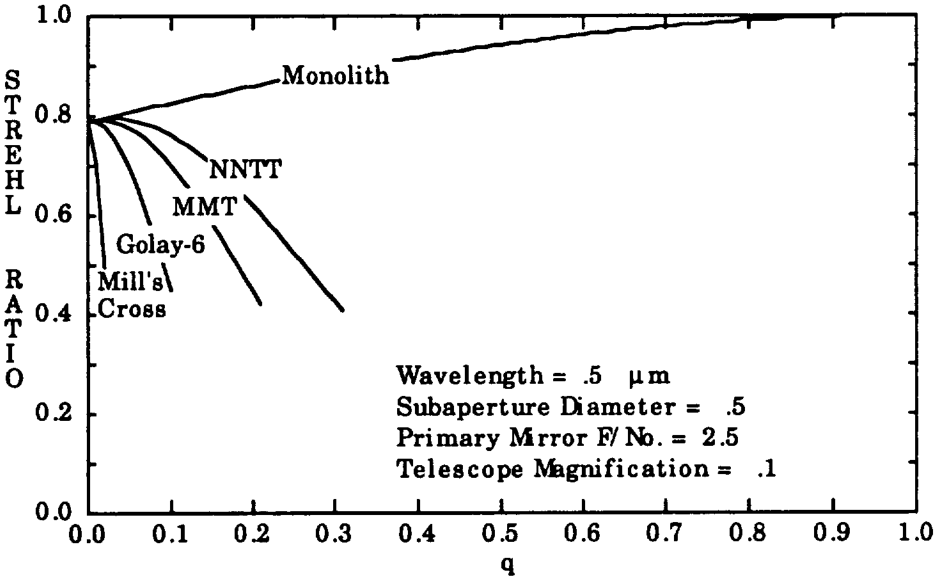

Figure 6-10. Strehl ratio vs. q for various subaperture configurations.

Note that, whereas the monolith improves monotonically as q goes from zero (flat focal plane) to unity (optimally curved focal surface for the monolith), the phased telescope arrays experience a slight improvement for small values of q followed by a very rapid decline in image quality. This phenomena is illustrated more clearly in the expanded view for small values of q provided in Figure 6-11.

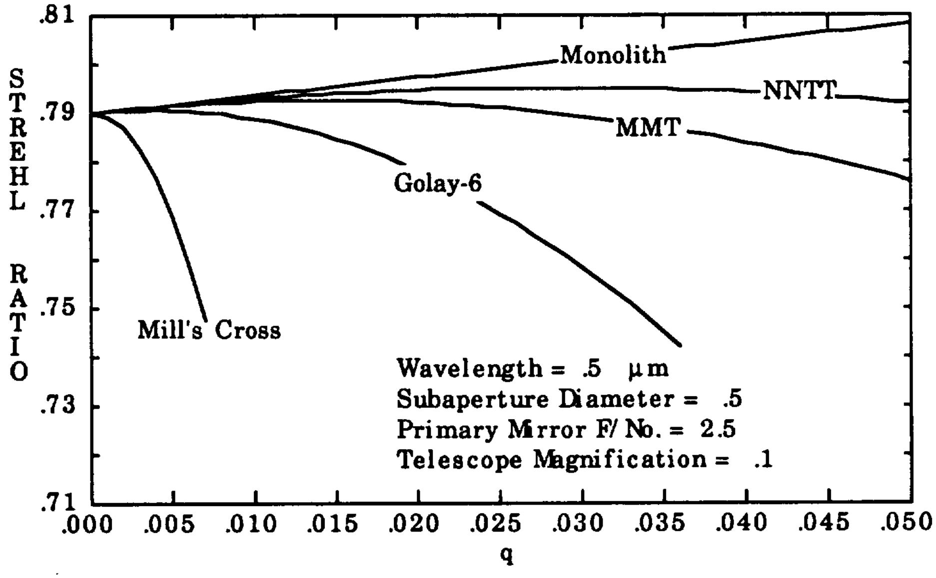

Figure 6-11. Strehl ratio vs. q illustrating that the maximum performance occurs at $q < 0.05$ for all phased array configurations studied.

It can be seen from both Table 6-1 and Figure 6-11 that the optimum focal surface for phased telescope arrays differs only very slightly from the flat focal plane, and only infinitesimal improvement is realized by going to a curved focal surface.

Incidentally, when we set q = 1, which corresponds to the analytical solution for Strehl ratio used in the previous section, we get excellent agreement between these two computational techniques. This is verified by comparing Figure 6-12 below with Figure 6-4.

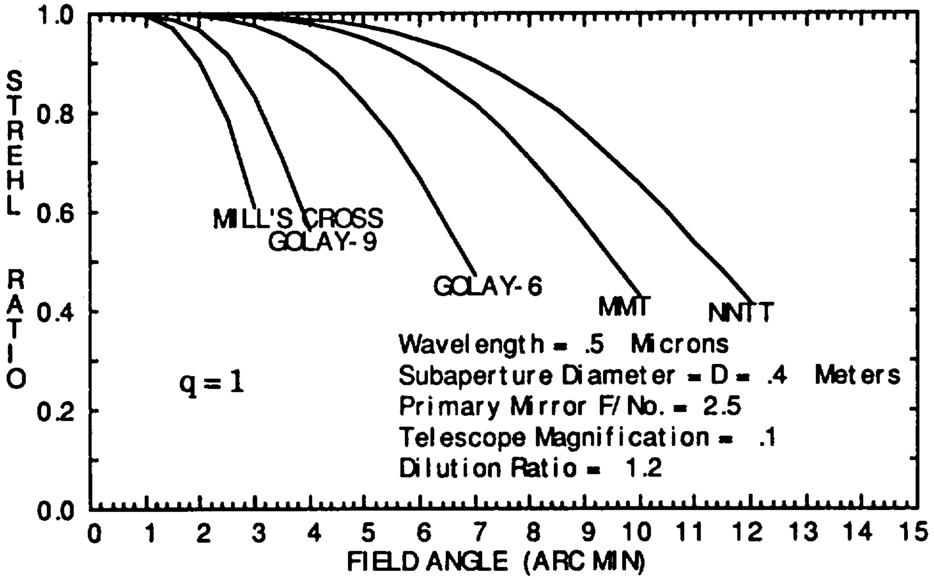

Figure 6-12. Calculations of Strehl ratio using the analytic solution for wavefront variance: to be compared to the results obtained by using the analytic solution for Strehl ratio exhibited in Figure 6-4.

We have seen that the analytical solution for wavefront variance expressed by Eq.(6-17) provides a great deal of insight into the way in which the subaperture configuration affects the optical performance of phased arrays of telescopes exhibiting field curvature. Furthermore, this equation can very easily be used to perform other parametric studies and sensitivity analyses.

6.3.3 Numerical Solution for Wavefront Variance

The third computational technique is the brute force numerical calculation of wavefront variance. This does not provide as much insight as the previous analytical solution; however, it is not limited to to a particular aberration such as field curvature.

For example, whatever the aberration might be, the wavefront variance can be calculated directly by numerically evaluating Eq.(6-15) which is repeated here for convenience

$$\sigma_w^2 = \overline{W^2} - \overline{W}^2 = (NA)^{-1}\iint W^2\, dx'\, dy' - [(NA)^{-1}\iint W\, dx'\, dy']^2 \qquad (6\text{-}27)$$

A listing of the numerical code is provided in Appendix E, and its output for the same input parameters as those used for Figure 6-4 and Figure 6-12 using the other two techniques is shown in Figure 6-13 below. A numerical sampling density sufficient to achieve the closed form solution to about 0.02% was used. The results are seen to be in excellent agreement with the results of the other two techniques.

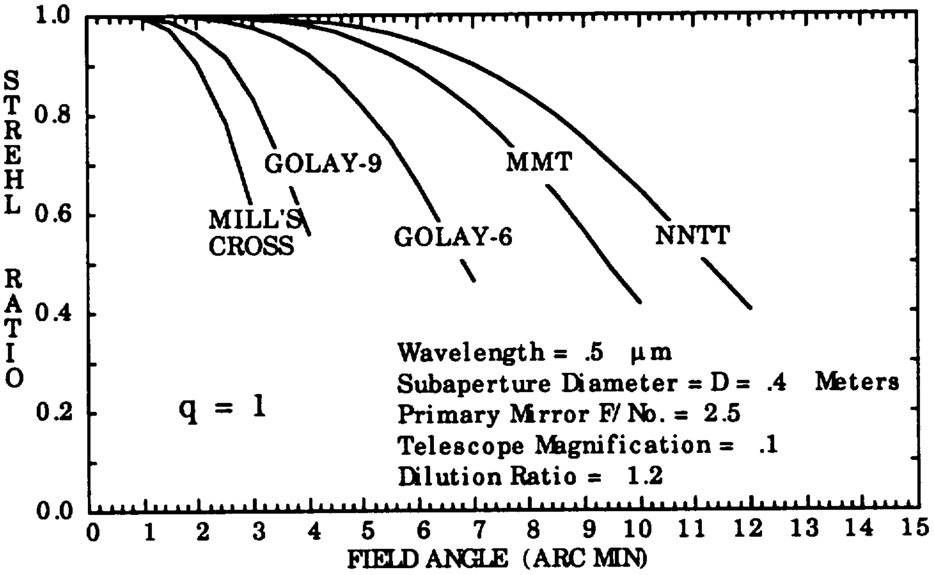

Figure 6-13. Numerical predictions of Strehl ratio for the same parameters used by the other two techniques: to be compared to results exhibited in Figure 6-4 and 6-12

These last two techniques are complementary and were both used to obtain results in the following parametric studies and sensitivity analyses.

6.4 PARAMETRIC RESULTS AND SENSITIVITY ANALYSES

Both techniques for determining wavefront variance can clearly be used to calculate Strehl ratio by merely applying Eq.(5-1) which is also repeated here

$$\text{Strehl ratio} = \exp[-(2\,\pi\,\sigma_w/\lambda)^2] \qquad (6\text{-}28)$$

Having two completely different computational techniques also provided a valuable check against each other. Excellent agreement between the two were observed in a variety of test cases.

6.4.1 Inherent Field Curvature of Two-mirror Telescopes

The following parametric performance predictions pertain to phased arrays of two-mirror telescopes that suffer from field curvature inherent to such designs. The magnitude of the field curvature coefficient for a Mersenne design is given by the primary mirror diameter, its F/no., the telescope magnification, and the field angle

$$\text{Field Curvature} = W_{20} = [\,D_p/(16\,F_p)]\,[(1-m)/m]\;\theta_o^2 \qquad (6\text{-}29)$$

We have previously shown that there is virtually nothing to be gained in terms of performance by going to a curved focal surface for phased telescope arrays; hence, the following parametric curves will all be for flat focal planes. We have also already shown that for a flat focal plane ($q = 0$), the wavefront variance and therefore the Strehl ratio will be the same for all subaperture configurations when the subaperture size is held fixed.

Figure 6-14 graphically illustrates image degradation expressed in terms of Strehl ratio as a function of field angle in arc minutes and its sensitivity to subaperture diameter. The wavelength is held constant at $\lambda = 0.5\ \mu m$, the primary mirror F/no. is set at 2.5, the telescope magnification is assumed to be 0.1, and the subaperture array dilution ratio is 1.2.

Recall that our error budget allocation for off-axis optical design errors corresponds to a Strehl ratio of 0.95. Notice from Figure 6-14 that subaperture diameters less than 0.4 meters will meet the error budget allocation for a semi-field angle of 15 arc minutes. For 1.0 meter diameter subapertures, the semi-field angle satisfying the error budget drops to approximately 3.5 arc minutes.

If the diameter of the telescopes making up the array is made even larger, the field-of-view within which the array will satisfy the established error budget allocation continues to drop rapidly. For example, Figure 6-15 shows that an array with four (4) meter diameter telescopes will perform satisfactorily over field angles of less than one-half arc minute, and eight (8) meter telescopes will yield a semi-field angle of only about ten (10) arc seconds.

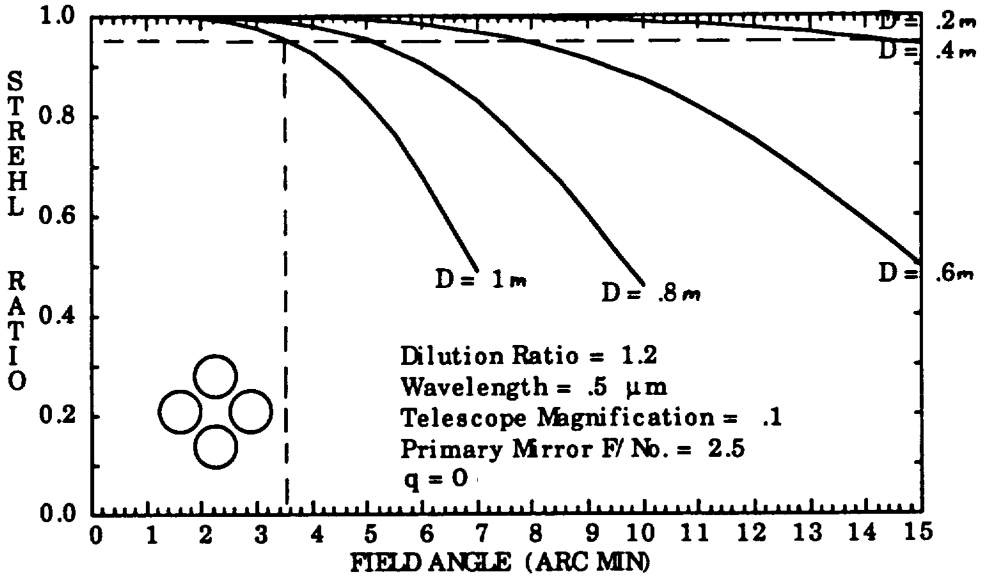

Figure 6-14. Sensitivity of Strehl ratio to subaperture diameter.

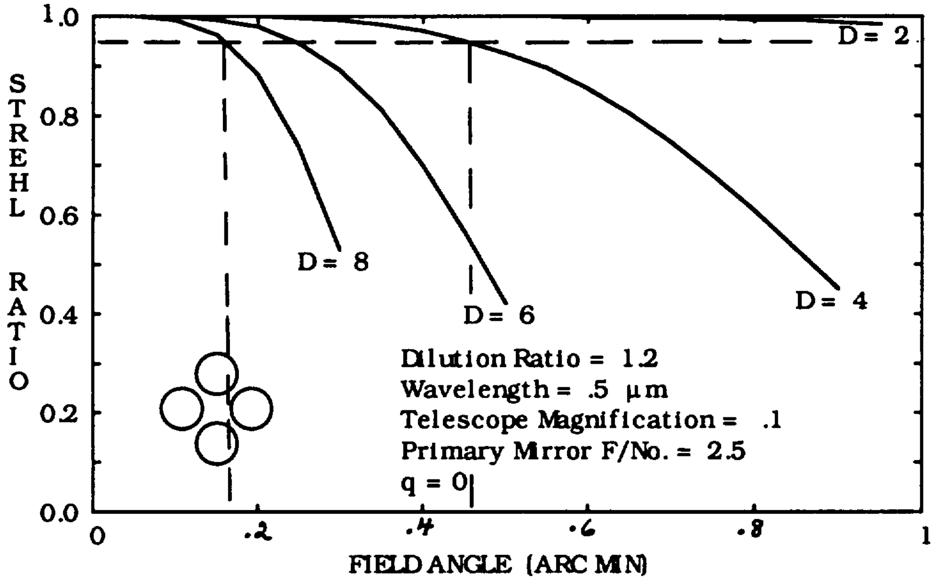

Figure 6-15. Sensitivity of Strehl ratio to subaperture size indicating sub arc minute FOV's for telescope diameters greater than two (2) meters.

It should also be evident that for a flat focal plane (q = 0), the wavefront variance and therefore the Strehl ratio will be the same for all dilution ratios when the subaperture size is held fixed. This fact was verified by making calculations for various dilution ratios which are observed to give identical results in Figure 6-16.

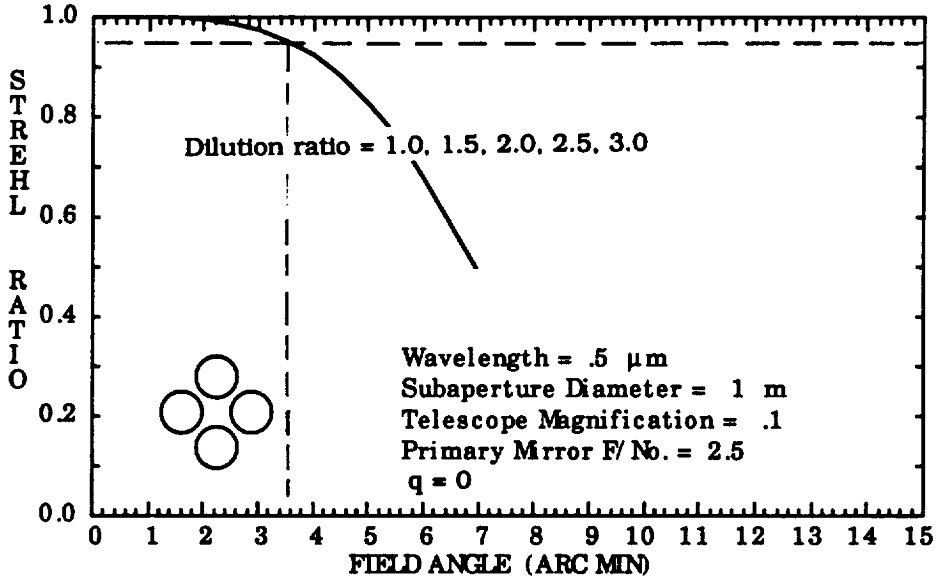

Figure 6-16. Strehl ratio is completely insensitive to dilution ratio.

Figures 6-17 and 6-18 demonstrate the sensitivity of FOV to telescope magnification and primary mirror F/no. respectively. Note that phased telescope arrays are relatively insensitive to modest changes in the F/no. of the primary mirror; however, changes in the telescope magnification can make a significant change in the useful FOV of the array. These parametric curves are all for two-mirror Mersenne telescope designs, uncorrected for field curvature.

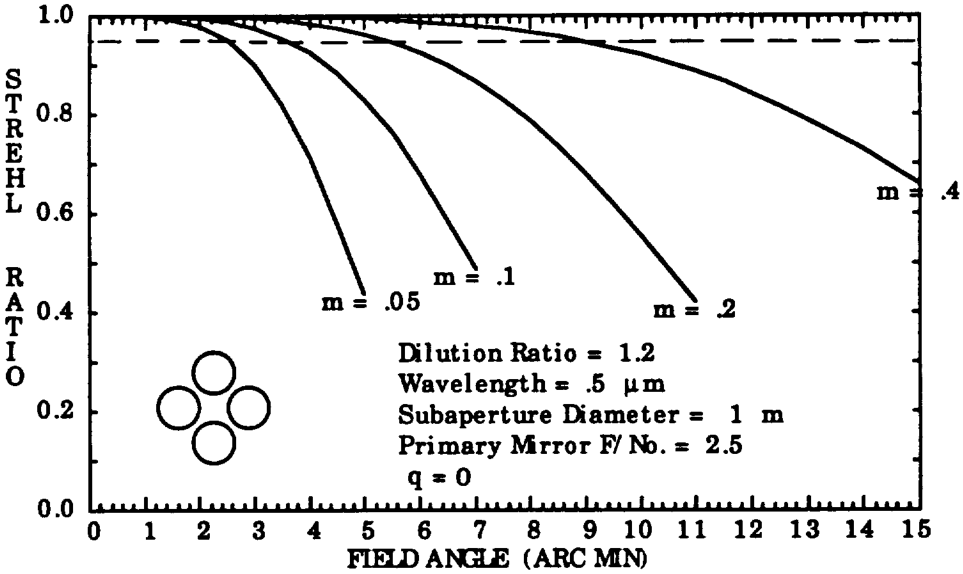

Figure 6-17. Sensitivity of Strehl ratio to telescope magnification

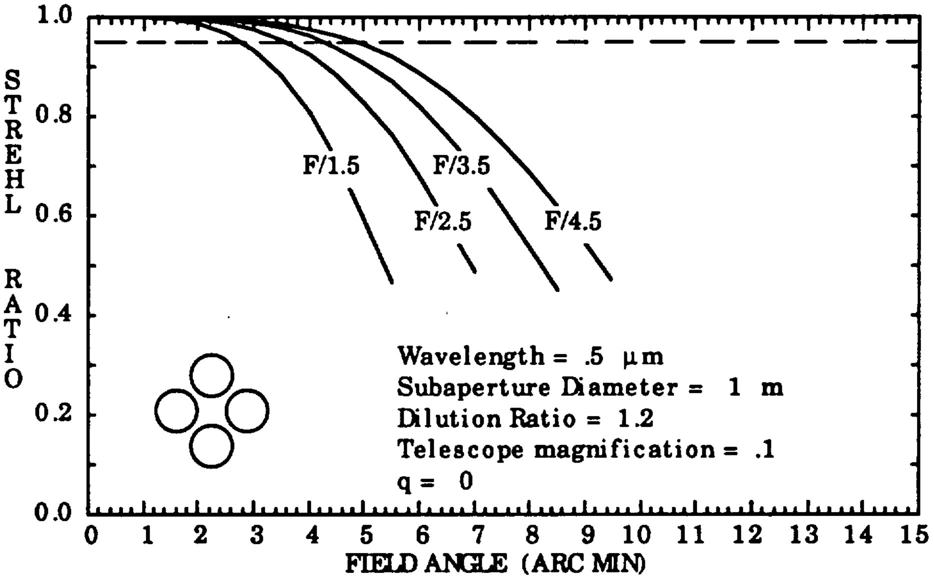

Figure 6-18. Sensitivity of Strehl ratio to primary mirror F/no.

A different perspective on the comparison between the subaperture configurations is obtained if we hold the total collecting area of the array constant rather than the diameter if the subapertures. Depending upon the application, this may be the more meaningful comparison. Figure 6-19 dramatically illustrates the superiority in FOV of using a larger number of smaller telescopes for equal area arrays.

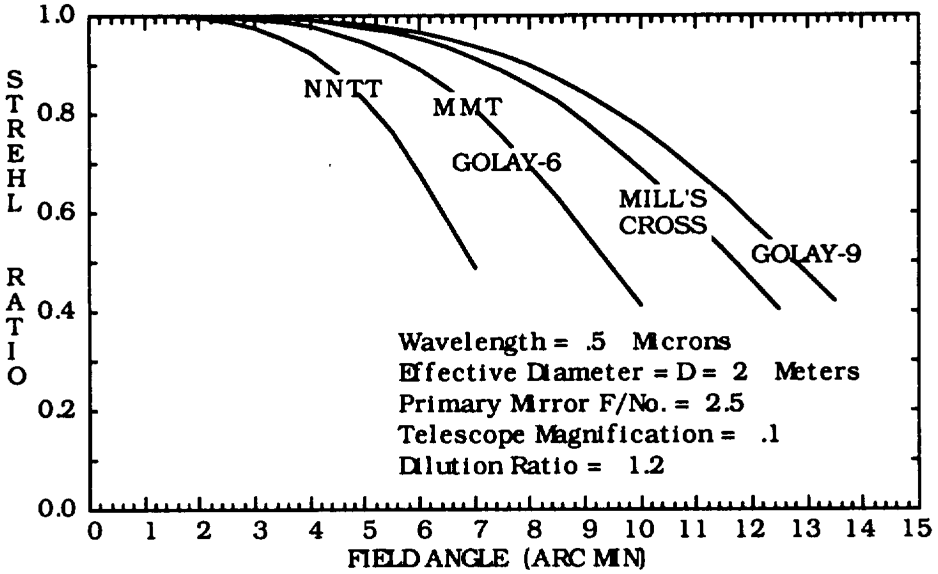

Figure 6-19. Sensitivity of Strehl ratio to subaperture configuration (Equal Area Arrays)

6.4.2 Residual Field Curvature of Corrected Systems

The previous parametric curves have indicated that, although a 15 arc minute FOV may be achieved with a 40 cm diameter laboratory working model of a phased array of two-mirror telescopes; the inherent field curvature of such designs will not allow them to be scaled up for large space applications. We now proceed to parametrically determine how well the field curvature must be corrected if a 0.5 degree FOV is to be achieved with a phased array made up of one (1) to four (4) meter diameter individual telescopes.

Figure 6-20 illustrates the predicted Strehl ratio at a field angle of 15 arc minutes as a function of the fractional residual field curvature after correction for a variety individual telescope sizes. For example, a phased array made up of two (2) meter diameter telescopes whose field curvature has been corrected to 0.0075 of its inherent value would just meet the error budget allocation of a 0.95 Strehl ratio at a field angle of 15 arc minutes. Similarly, a phased array made up of four (4) meter diameter telescopes will meet the requirement if the F. C. is corrected to slightly better than 0.001 of its inherent uncorrected value.

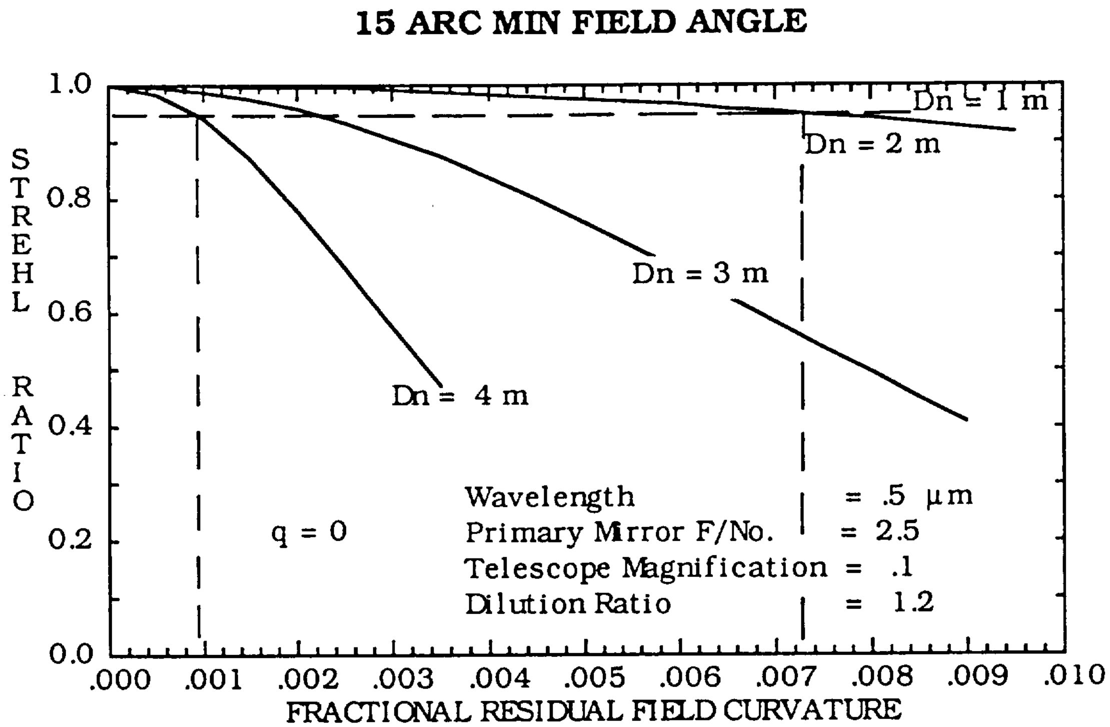

Figure 6-20. Improved performance of field-flattened telescope designs

6.4.3 Distortion due to Two-mirror Telescopes

In the last section we showed that field curvature can probably be sufficiently well corrected to not be a dominant error source preventing wide-field imaging with phased telescope arrays. We must now look at the next term in the aberration expansion shown previously in Eq.(6-2). Third-order distortion in the individual telescopes will have the form

$$W_n(x, y) = W_{11}\ r \cos\psi \ = W_{11}\ y \qquad (6\text{-}30)$$

However, from Figure 6-3 we see that when we go to the array coordinate system, $y = y' - y_n$, and

$$W_n(x', y') = W_{11}\ (y' - y_n) \qquad (6\text{-}31)$$

hence, for the entire array

$$W(x', y') = \underbrace{\sum_{n=1}^{N} W_{11}\ y'\ \mathrm{cyl}[(r' - r_n)/D]}_{\text{Conventional Distortion}} - \underbrace{\sum_{n=1}^{N} W_{11}\ y_n\ \mathrm{cyl}[(r' - r_n)/D]}_{\text{Relative Piston Errors}} \qquad (6\text{-}32)$$

Recall from Eq.(6-4) that

$$W_{11} = (D_p/8)\ [(3m + 1)(m - 1)/m^2]\ \theta^3 \qquad (6\text{-}33)$$

As before, the wavefront variance is given by

$$\sigma_w^2 = \overline{W^2} - \overline{W}^2 = (NA)^{-1}\iint_{-\infty}^{\infty} W^2\ dx'\ dy' - [(NA)^{-1}\iint_{-\infty}^{\infty} W\ dx'\ dy']^2 \qquad (6\text{-}34)$$

and calculated by the numerical technique discussed earlier. The Strehl ratio is then determined from Eq.(5-1)

$$\text{Strehl ratio} = \exp[-(2\ \pi\ \sigma_w/\lambda)^2\ ] \qquad (6\text{-}35)$$

and plotted versus field angle for different design parameters. Figure 6-21 illustrates the predicted Strehl ratio versus field angle for different subaperture diameters. For the design parameters indicated (F/2.5, m=0.1 telescopes with dilution ratio of 1.2 operating at $\lambda = 0.5\ \mu m$), the third-order distortion inherent to a two-mirror telescope would limit the semi field angle to less than 10 arc min for 0.5 m diameter telescopes, to about 6 arc min for 1.0 m diameter telescopes, and to less than 4 arc min for 2.0 m telescopes. It is therefore clear that distortion must also be corrected if a 0.5 degree FOV is to be achieved with phased arrays of large telescopes.

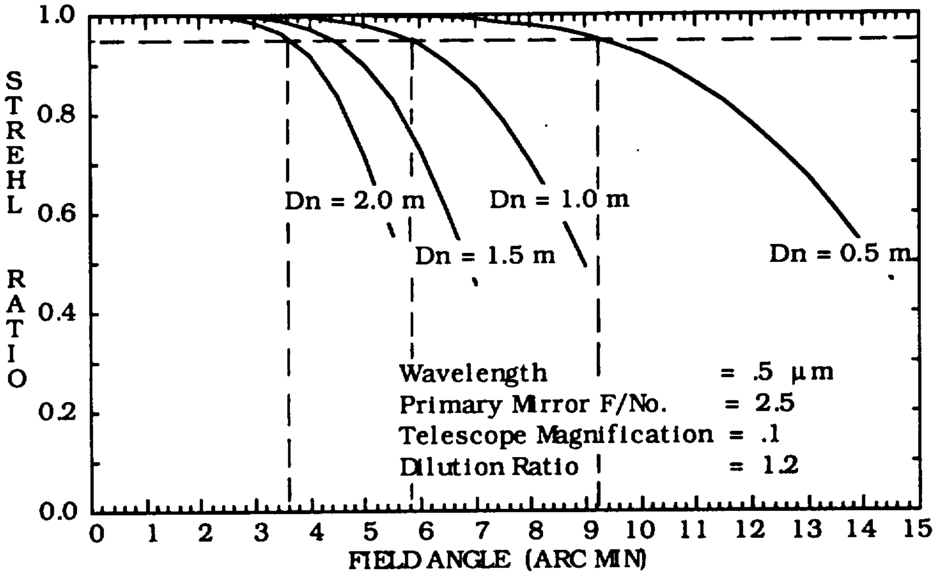

Figure 6-21. Field-of-view limitation due to uncorrected distortion.

The image degradation due to third-order field curvature is again independent of subaperture configuration. And the numerical calculations illustrated above have been shown to agree with an analytical solution for Strehl ratio.

Figure 6-22 illustrates the degree to which third-order distortion must be corrected in order to achieve a 0.5 degree FOV for large telescope diameters.

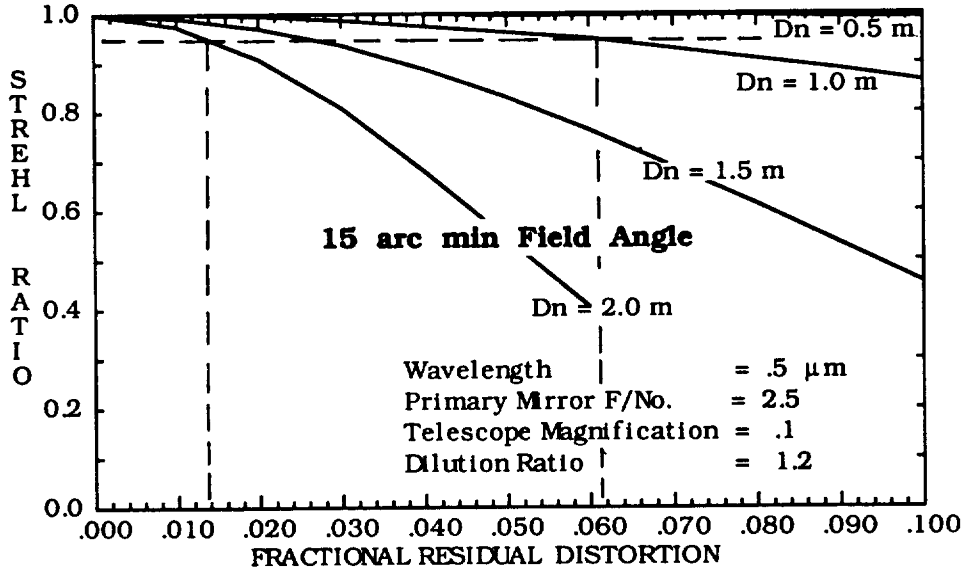

Figure 6-22. Strehl ratio vs. fractional residual distortion.

If distortion is corrected to 0.1 of its inherent value for a Mersenne design, a phased array made up of 0.5 meter diameter telescopes is well within our error budget, one (1.0) meter diameter telescopes must be corrected to a fractional residual distortion of 0.06, and two (2.0) meter diameter telescopes must be corrected to a fractional residual distortion of almost 0.01.

7.0 THE AFWL MULTIPURPOSE MULTIPLE TELESCOPE TESTBED

The AFWL Multipurpose Multiple Telescope Testbed (MMTT) illustrated in Figure 7-1 consists of four Cassegrain telescopes 20 cm in diameter positioned in the NNTT configuration 25 cm apart (Dilution ratio = 1.25). The telescopes have a magnification of 0.1 with F/1.8 primary mirrors. Note that field flattening lenses have been incorporated along with a superachromat re-collimating lens. In addition, a weak zoom lens is used to allow manual adjustment of the telescope magnification. It should also be pointed out that the axial pupil mapping errors can be adjusted by axially positioning the field flattening lens. This design is discussed in detail in References 14 and 29.

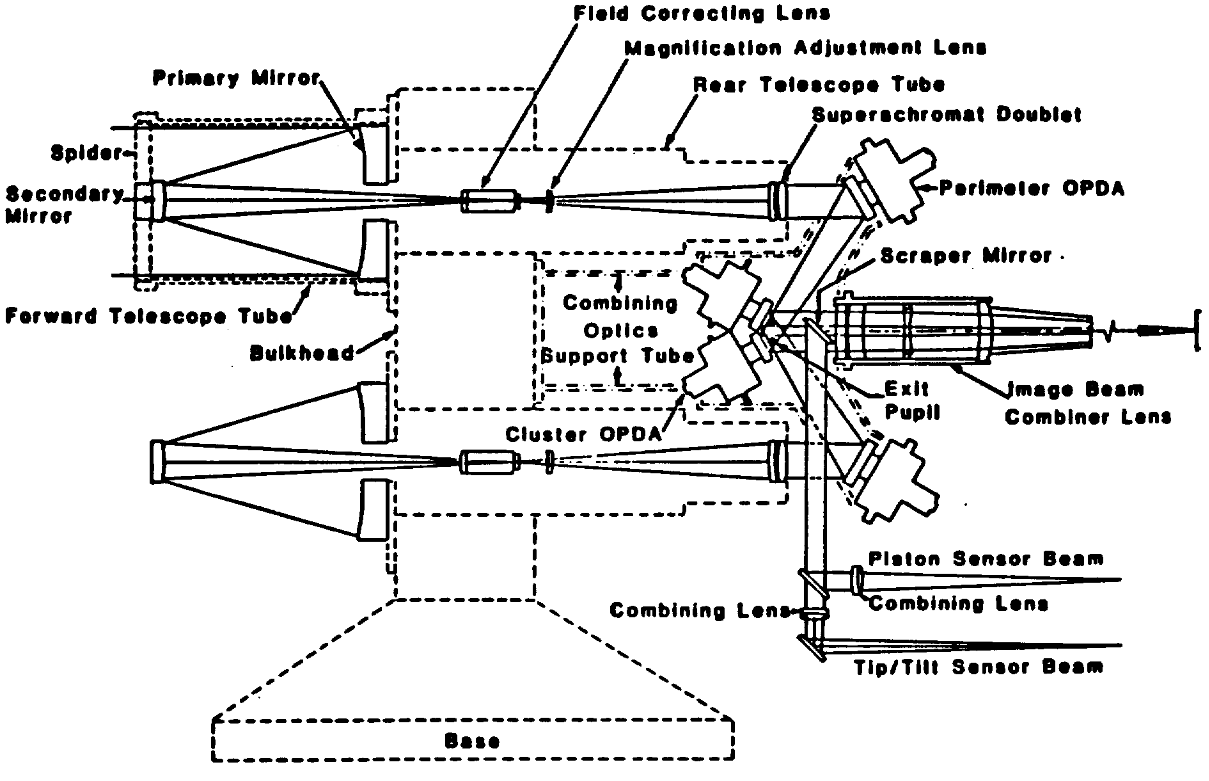

Figure 7-1. Schematic diagram of the AFWL MMTT

Preliminary analysis of the effects of <u>uncorrected field curvature</u> (no field lens) of the independent telescopes upon the phased telescope array performance for these design parameters is indicated in Figure 7-2 as the telescopes are scaled up in size. The 20 cm diameter telescopes introduce insignificant image degradation for field angles less than 15 arc min. Forty centimeter diameter telescopes would perform within the error budget out to a field angle of 12.5 arc minutes and one meter diameter telescopes would have a semi FOV of three (3) arc minutes.

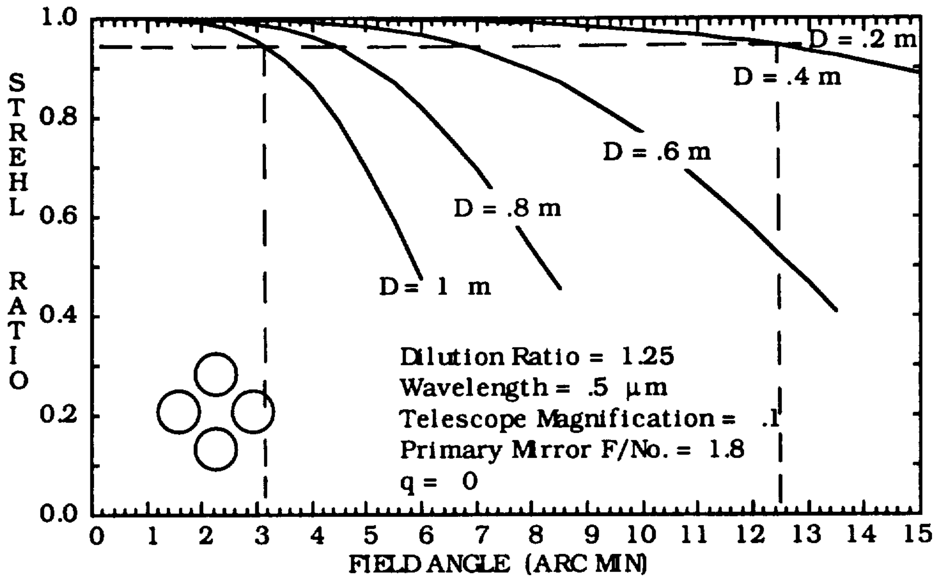

Figure 7-2. Strehl ratio of the MMTT design parameters due to uncorrected field curvature as it is scaled up in size.

If the field curvature in merely corrected to 0.2 of its uncorrected value, Figure 7-3 shows that we can scale the system up in size to 60 cm diameter subapertures and still meet the performance goal of a Strehl ratio of 0.95 at the design goal of 15 arc minute field angles. If the MMTT design were scaled up to 1.0 meter diameter subapertures, the field curvature would have to be corrected to approximately 0.04 of its uncorrected value.

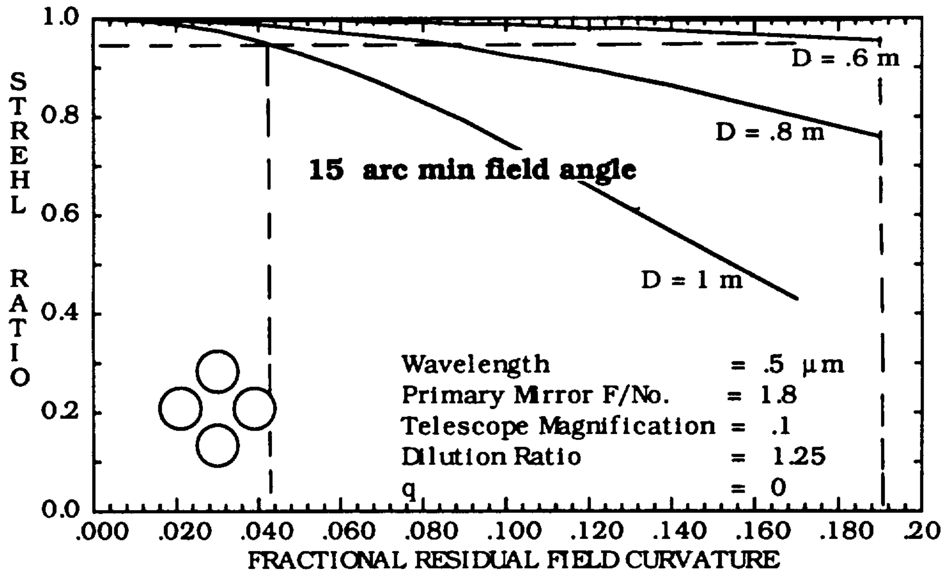

Figure 7-3. A 1/2 degree FOV can be achieved for telescope diameters up to one meter with modest correction of field curvature.

Applications requiring large phased arrays in space are feasible if truly flat-field telescope designs are used. Figure 7-4 illustrates that a phased array of four (4.0) meter diameter telescopes would have to be corrected to a residual field curvature of approximately 0.0006 times its uncorrected value if a one-half degree FOV is required.

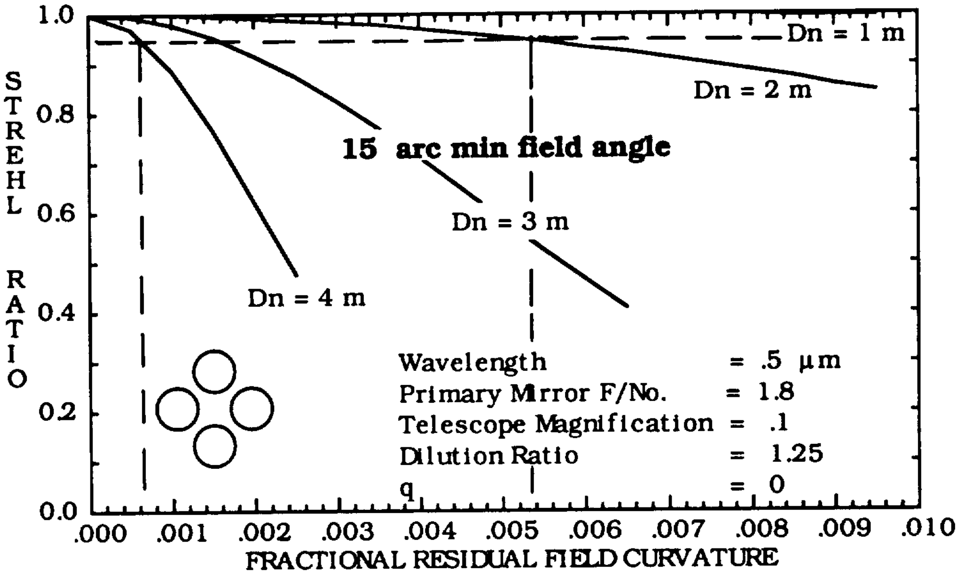

Figure 7-4. Strehl ratio of a large MMTT design as a function of fractional residual field curvature.

With field curvature highly corrected, the dominant source of image degradation due to the off-axis aberrations of the individual telescopes will be from distortion. Figure 7-5 illustrates the predicted Strehl ratio versus field angle for a phased array due to distortion of the individual telescopes. The twenty (20) centimeter diameter telescopes used in the AFWL MMTT should not need to be corrected for distortion in order to achieve a one-half degree FOV; however, forty (40) centimeter diameter telescopes would only perform satisfactorily within an eleven (11) arc min field angle, and a phased array made up of one (1) meter diameter telescopes would only meet the error budget for field angles up to 6 arc minutes.

Therefore, if wide fields-of-view are to be achieved with phased arrays of large telescopes, even distortion must be corrected in the individual telescopes. Figure 7-6 illustrates the predicted Strehl ratio at a 15 arc minute field angle versus the fractional residual distortion for telescope sizes ranging up to two (2) meters in diameter. One (1) meter diameter telescopes must be corrected to a fractional residual distortion of 0.06 and two (2) meter diameter telescopes would need to have distortion corrected to 0.01 of its inherent value if our error budget is to be satisfied.

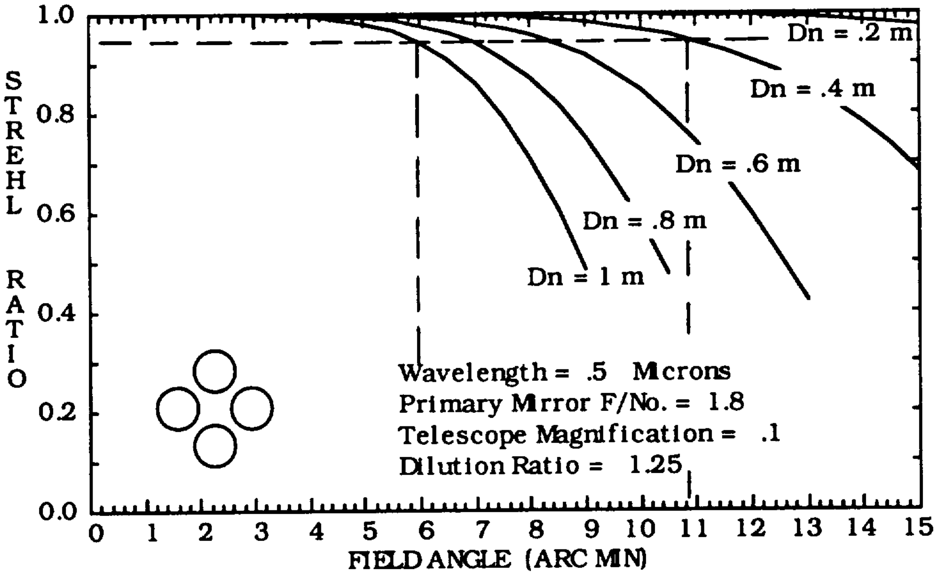

Figure 7-5. Predicted Strehl ratio vs. field angle due to distortion in the MMTT design for various telescope diameters.

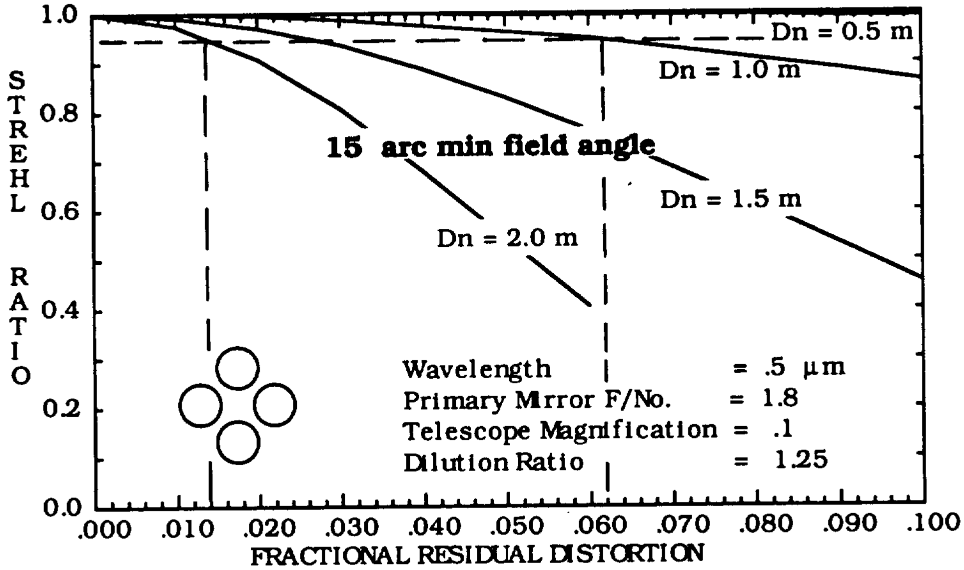

Figure 7-6. Predicted Strehl ratio vs. fractional residual distortion in the MMTT design for various telescope diameters.

8.0 SUMMARY AND CONCLUSIONS

~~We have~~ considered the problems encountered in obtaining a wide field-of-view (0.5 degrees) with large, space-based direct imaging phased telescope arrays. After defining some of the critical systems issues, we reviewed and summarized previous relevant work in the literature. Residual optical design errors (off-axis aberrations) of the individual telescopes making up the array stood out as a fundamental limitation largely unexplored to date.

We then made an extensive list of potential error sources and categorized them in the form of an error budget tree including optical design errors, optical fabrication errors, assembly and alignment errors, and environmental errors. After choosing a top level image quality requirement as a goal, we first performed a preliminary tops-down error budget allocation; then, based upon engineering experience, detailed analysis, or data from the literature, we performed a bottoms-up error budget reallocation in an attempt to achieve an equitable distribution of difficulty in satisfying the various allocations. This exercise provided us with a realistic allocation for residual off-axis optical design errors ($\sigma_W < 0.0375\ \lambda$) in the presence of state-of-the-art (Hubble Space Telescope) optical fabrication and alignment errors.

Previous work by the author describing the diffraction-limited performance of phased telescope arrays, complete with calculated PSF profiles and encircled energy plots, was referenced and attached as an Appendix. The effects of telescope aberrations upon phased array performance was then discussed in detail and it was shown that the somewhat benign (for conventional optical systems) aberrations of field curvature and distortion result in field dependent relative phase (piston) and pointing (tilt) errors which rapidly degrade the image quality as the field-of-view is increased.

Three different computational techniques were developed for computing the image degradation of phased telescope arrays due to the aberrations of the individual telescopes: 1.) an analytical expression for the Strehl ratio was derived for field curvature and distortion; 2.) an analytical expression for the rms wavefront error, σ_W, was derived for the case where field curvature is the dominant aberration present; and 3.) a computer code was developed to numerically calculate the rms wavefront error in the presence of arbitrary aberrations. Previously reported results based upon an incorrect implementation of technique No. 1.) were found to be overly pessimistic. These predictions were corrected and verified by technique No. 2.), and the relaxed requirements were determined. Technique No. 2.) was found to provide a great deal of insight concerning the optimally curved focal surface and the variation (or lack thereof) in performance for different subaperture configurations. A flat focal surface is almost optimum, and, for that flat focal surface, there is no difference in the image degradation due to field curvature for different configurations. All three computational techniques were tested against each other and found to yield identical results for given test cases.

Parametric studies and sensitivity analyses were then performed for a variety of subaperture configurations and telescope design parameters in an attempt to determine how the off-axis performance of a phased telescope array varies as the telescopes are scaled up in size. It was quickly learned that the inherent field curvature of two-mirror telescopes will prevent attaining a 0.5 degree field-of-view for individual telescope diameters greater than about forty (40) centimeters. A phased array made up of four (4) meter telescopes will satisfy the error budget only for field angles less than about one-half (1/2) arc minute, and eight (8) meter telescopes will perform satisfactorily only for semi field angles less than about ten (10) arc seconds.

With flat-field telescope designs, third-order distortion will still prevent the individual telescopes from being scaled up to the two to four meter sizes of interest. Specific telescope designs which are corrected for both field curvature and distortion must thus be developed if wide-field, large space-based phased telescope arrays are to become a reality.

The AFWL MMTT configuration was analyzed in detail with regard to image degradation due to field curvature and distortion of the individual telescopes as they are scaled up in size. The twenty (20) centimeter telescopes of the MMTT are corrected for field curvature well beyond that required for a one-half degree field-of-view. The uncorrected distortion for the MMTT introduces about one-half of the allowable image degradation according to the preliminary error budget established in this study.

9.0 REFERENCES

1. A. B. Meinel, "Aperture Synthesis Using Independent Telescopes", Appl. Opt. **9**, 2501 (1970).

2. G. M. Sanger, "The Techniques and Tolerancing Required for Phasing Hexagonally-Configured Synthetic Aperture Imaging Systems", Ph.D. Dissertation, University of Arizona (1976).

3. Wesley A. Traub, "Combining Beams from Separated Telescopes", Appl. Opt. **25**, 528 (1986).

4. Jacques M. Beckers, "Field of View Considerations for Telescope Arrays", SPIE Proceedings Vol. 628, 255 (1986).

5. J. E. Harvey, Alan B. Wissinger, and Alan N. Bunner, "A Parametric Study of Various Synthetic Aperture Telescope Configurations for Coherent Imaging Applications", SPIE Proceedings Vol. 643, 194 (1985).

6. J. W. Goodman, *Introduction to Fourier Optics*, McGraw-Hill, New York (1968).

7. David E. Stoltzman, "The Perfect Point Spread Function", *Applied Optics and Optical Engineering*, Volume IX, page 111, Academic Press (1983).

8. R. R. Butts, S. J. Cusumano, J. S. Fender, and C. R. DeHainaut, "Phasing Concept for an Array of Mutually Coherent Laser Transmitters", Opt. Eng. Vol. 26, No. 6, page 553 (1987).

9. R. R. Butts, "Analysis of Phase Measurement Algorithms Utilizing Two-beam Interference", SPIE Proceedings Vol. 440, 130 (1983).

10. R. A. Carreras, S. J. Cusumano, M. G. Andrews, and D. H. Jordan, "Overview of a Phased Array Experiment", SPIE Proceedings Vol. 440, 168 (1983).

11. J. S. Fender, "Phased Array Optical Systems", SPIE Proceedings Vol. 643, 122 (1983).

12. J. S. Fender and R. A Carreras, "Demonstration of an Optically Phased Telescope Array", Opt. Eng. Vol. 27, No. 9, page 706 (1988).

13. L. D. Weaver, J. S. Fender, and C. R. DeHainaut, "Design Considerations for Multiple Telescope Imaging Arrays", Opt. Eng. Vol. 27, No. 9, 730 (1988).

14. C. R. DeHainaut, K. P. Hentz, L. D. Weaver, and J. D. Gonglewski, "Design of a Wide Field of View Phased Array Telescope", Opt. Eng. Vol. 17, No. 9, page 736 (1988).

15. A. B. Meinel *et al.*, "Multiple Aperture Telescope Diffraction Images", *Applied Optics and Optical Engineering*, Volume IX, pages 149-201, Academic Press (1983).

16. J. E. Harvey and R. A. Rockwell, "Performance Characteristics of Phased Array and Thinned Aperture Optical Telescopes", Opt. Eng. Vol. 27, No. 9, page 762 (1988).

17. M. J. E. Golay, "Point Arrays Having Compact Non-redundant Autocorrelations", J.O.S.A. 61, 272 (1971).

18. Alan B. Wissinger *et al.*, "Final Study Report for Astronomical Interferometric System Technology Requirements (AISTR) Study", Perkin-Elmer ER-991, prepared for NASA/MSFC, June 1986.

19. R. R. Butts, "Effects of Piston and Tilt Errors on the Performance of Multiple Mirror Telescopes", SPIE Proceedings Vol. 293 (1981).

20. D. G. Voelz, D. A. Russell, P. J. Wallentine and R. A. Carreras, "Implementation of Optical Path Length and Tilt Control in a Phased Array System", Appl. Opt. Vol. 27, No. 9, 712 (1988).

21. Karl P. Hentz, "Multiple Beam Combination with Pupil Geometry Maintenance", Appl. Opt. Vol. 27, No. 9, 740 (1988).

22. H. H. Hopkins, *Wave Theory of Aberrations*, Oxford Press, New York (1950).

23. V. N. Mahajan, "Strehl Ratio for Primary Aberrations in terms of their Aberration Variance", J.O.S.A. Vol. 73, No. 6, 860 (1983).

24. HST Report, "OTA Error Budget Report", Perkin-Elmer PR-182D (1985).

25. SOT Report, "Sot Conceptual Design & Cost Review", Perkin-Elmer ER SOT-146 (1984).

26. James E. Harvey, Malcolm J. MacFarlane, and James L. Forgham, "Design and Performance of Ranging Telescopes: Monolithic Versus Synthetic Aperture", Optical Engineering Vol. 24, No. 1, 183 (1985).

27. R. V. Shack, "The Use of Normalization in the Application of Simple Optical Systems", SPIE Proceedings Vol. 54 (1974).

28. J. D. Gaskill, *Linear Systems, Fourier Transforms, and Optics*, John Wiley and Sons, New York (1978).

29. C. M. Lampkin, G. W. Flint, and M. J. MacFarlane, "Optical and mechanical design aspects of a four-telescope array for combined imaging", Appl. Opt. Vol. 27, No. 9, 749 (1988).

APPENDIX D

Analytical Solution for Wavefront Variance of Phased Arrays due to Field Curvature of Individual Telescopes

This Appendix provides the detailed derivation of Equation (6-17) in this report which expresses wavefront variance for phased arrays of identical independent telescopes exhibiting field curvature in terms of the subaperture configuration and a parameter determined by the curvature of the final focal surface.

Analytical Solution for Wavefront Variance of Phased Arrays due to Field Curvature of Individual Telescopes

In a phased telescope array, the field curvature of the individual telescopes results in a wavefront error over the nth subaperture (in its own coordinate system) given by

$$W_n(x, y) = W_{20}\ r^2 = W_{20}\ (x^2 + y^2) \tag{1}$$

The array coordinates are given by (see Figure 6-3 in the main body of the report)

$$x' = x_n + x, \text{ and } y' = y_n + y \tag{2}$$

where x_n and y_n are the coordinates of the nth subaperture, hence

$$W_n(x', y') = W_{20}\ [(x' - x_n)^2 + (y' - y_n)^2] \tag{3}$$

This equation can be rewritten as

$$W_n = W_{20}\ r_n^2 - 2\ W_{20}\,(x'\ x_n + y'\ y_n) + W_{20}\ r'^2 \tag{4}$$

The first term is a relative phase (piston) error between the various subapertures and the second term is a relative wavefront tilt (or pointing error) between the subapertures. These two terms can rapidly degrade image quality for increasing field angles thus severely limiting the useful field of view of the phased telescope array. The third term is a conventional field curvature for the array which can be partially compensated by utilizing a curved focal surface for the beam combining telescope.

If we sum the contributions of the wavefront error described in Eq.(4) over the subapertures making up the array, and add an arbitrary amount of array field curvature (W_{20}') corresponding to a curved focal surface in the beam combining telescope, we obtain the following expression for the wavefront error for the entire array

$$W = \sum_{n=1}^{N} W_n\ r^2\ C_n - \sum_{n=1}^{N} W_{20}'\ r'^2\ C_n \tag{5}$$

where

$$C_n = \mathrm{cyl}[(r' - r_n)/D] \tag{6}$$

is a shifted cylinder (tophat) function of diameter D as defined by Gaskill.[28]

When we substitute Eq. (4) into Eq.(5) and rearrange, we obtain

$$W = \sum_{n=1}^{N} W_{20}\, r_n^2\, C_n - \sum_{n=1}^{N} 2\, W_{20}\, (x_n x' + y_n y')\, C_n + \sum_{n=1}^{N} (W_{20} - W_{20}')\, r_n'^2\, C_n \qquad (7)$$

Factoring out W_{20} and setting

$$q = W_{20}'/W_{20} \qquad (8)$$

we obtain

$$W = W_{20}\, \Big[\sum_{n=1}^{N} r_n^2\, C_n - 2 \sum_{n=1}^{N} (x_n x' + y_n y')\, C_n + (1 - q) \sum_{n=1}^{N} r_n'^2\, C_n\Big] \qquad (9)$$

but since $x' = x_n + x$, $y' = y_n + y$, and $r'^2 = x'^2 + y'^2$

$$W = W_{20}\, \Big[\sum_{n=1}^{N} r_n^2\, C_n - 2 \sum_{n=1}^{N} (r_n^2 + x_n x + y_n y)\, C_n$$

$$+ (1 - q) \sum_{n=1}^{N} (r_n^2 + 2\, x_n x + 2\, y_n y + r^2)\, C_n\Big] \qquad (10)$$

Collecting similar terms

$$W = W_{20}\, \Big[(1 - q) \sum_{n=1}^{N} r^2\, C_n - q \sum_{n=1}^{N} r_n^2\, C_n - q \sum_{n=1}^{N} 2\, (x_n x + y_n y)\, C_n\Big] \qquad (11)$$

We now proceed to calculate the wavefront variance

$$\sigma_w^2 = \overline{W^2} - \overline{W}^2 = (NA)^{-1} \iint_{-\infty}^{\infty} W^2\, dx'\, dy' - \Big[(NA)^{-1} \iint_{-\infty}^{\infty} W\, dx'\, dy'\Big]^2 \qquad (12)$$

where N is the number of subapertures and

$$A = \text{area of subaperture} = \pi D^2/4 = \pi r_0^2 . \qquad (13)$$

Noting that $dx' = dx$, $dy' = dy$ the second term in Eq.(12) can now be written as

$$\overline{W}^2 = \Big[(W_{20}/NA)\Big[(1 - q) \sum_{n} \underbrace{\iint_{-\infty}^{\infty} r^2\ \ C_n\, dx\, dy}_{A} \qquad (14)$$

$$- q \sum_{n} r_n^2 \iint_{-\infty}^{\infty} C_n\ dx\, dy - 2\, q \underbrace{\sum_{n} \iint_{-\infty}^{\infty} (x_n x + y_n y)\, C_n\ dx\, dy}_{0}\Big]^2$$

This can now be written as

$$\overline{W}^2 = \left[(W_{20}/NA)[(1-q)\sum_n \int_{\phi=0}^{2\pi}\int_{r=0}^{r_0} r^3\ dr\, d\phi\ - q\ NA\,(1/N)\sum_n r_n^2\ ]\right]^2 \qquad (15)$$

$$\overline{W}^2 = \left[(W_{20}/NA)[(1-q)\ 2\pi\, r_0^4/4\ - q\ NA\ \overline{r_n^2}\ ]\right]^2 \qquad (16)$$

$$\overline{W}^2 = \left[W_{20}\,[(1-q)\ r_0^2/2\ - q\,\overline{r_n^2}\ ]\right]^2 \qquad (17)$$

Factoring out $(W_{20}\ r_0^2)^2$

$$\overline{W}^2 = (W_{20}\ r_0^2)^2\left[q^2\ \overline{(r_n/r_0)^2}^{\,2} - q\,(1-q)\ \overline{(r_n/r_0)^2}\ -\ (1-q)^2/4\ \right] \qquad (18)$$

Squaring Eq.(11) we obtain

$$\begin{aligned} W^2 = W_{20}^{\ 2}\Big[&(1-q)^2\ r^4\sum_{n,m} C_n C_m - 2\,q\,(1-q)\,r^2\sum_{n,m} r_n^2\ C_n C_m \\ &-\ 4\,q\,(1-q)\,r^2\sum_{n,m}(x_n x + y_n y)\,C_n C_m\ + q^2\sum_{n,m} r_n^2\, r_m^2\, C_n C_m \qquad (19) \\ &+\ 4\,q^2\sum_{n,m} r_n^2\,(x_n x + y_n y)\,C_n C_m\ + 4\,q^2\sum_{n,m}(x_n x + y_n y)(x_m x + y_m y)\,C_n C_m\Big] \end{aligned}$$

But $C_n C_m = \delta_{nm}\ C_n$, hence

$$\begin{aligned} W^2 = W_{20}^{\ 2}\Big[&(1-q)^2\ r^4\sum_n C_n\ - 2\,q\,(1-q)\,r^2\sum_n r_n^2\ C_n \\ &-\ 4\,q\,(1-q)\,r^2\sum_n(x_n x + y_n y)\,C_n\ + q^2\sum_n r_n^4\ C_n \qquad (20) \\ &+\ 4\,q^2\sum_n r_n^2\,(x_n x + y_n y)\,C_n\ + 4\,q^2\sum_n(x_n x + y_n y)^2\ C_n\Big] \end{aligned}$$

The first term of Eq.(12) can now be written as

$$\begin{aligned} \overline{W^2} = (W_{20}^{\ 2}/NA)\Big[&(1-q)^2\sum_n\iint_{-\infty}^{\infty} r^4\ C_n\ dx\,dy - 2\,q(1-q)\sum_n r_n^2\iint_{-\infty}^{\infty} r^2\ C_n\,dx\,dy \\ &-\ 4\,q\,(1-q)\underbrace{\sum_n\iint_{-\infty}^{\infty} r^2\ (x_n x + y_n y)\,C_n\,dx\,dy}_{0}\ + q^2\sum_n r_n^4\underbrace{\iint_{-\infty}^{\infty} C_n\ dx\,dy}_{A} \qquad (21) \\ &+\ 4\,q^2\sum_n r_n^2\underbrace{\iint_{-\infty}^{\infty}(x_n x + y_n y)\,C_n\,dx\,dy}_{0}\ + 4\,q^2\sum_n\iint_{-\infty}^{\infty}(x_n x + y_n y)^2\ C_n\ dx\,dy\Big] \end{aligned}$$

Rewriting, we obtain

$$\overline{W^2} = (W_{20}{}^2/NA)\Big[(1-q)^2\ NA\ r_0^4/3 - 2\ q(1-q)\ 2\ NA\ (r_0^4/4)(1/N)\sum_n r_n^2 + q^2\ NA\ (1/N)\sum_n r_n^4 + 4\ q^2 \sum_n \Big[x_n^2 \underbrace{\iint_{-\infty}^{\infty} x^2\ C_n\, dx\, dy}_{A\, r_0^2/4} + y_n^2 \underbrace{\iint_{-\infty}^{\infty} y^2\ C_n\, dx\, dy}_{A\, r_0^2/4} + x_n y_n \underbrace{\iint_{-\infty}^{\infty} x\, y\, C_n\, dx\, dy}_{0}\Big]\Big] \qquad (22)$$

Finally

$$\overline{W^2} = W_{20}{}^2\big[(1-q)^2\ r_0^4/3 - q(1-q)\ r_0^2\ \overline{r_n^2} + q^2\ \overline{r_n^4} + q^2\ r_0^2\ \overline{r_n^2}\big] \qquad (23)$$

Factoring out r_0^4

$$\overline{W^2} = (W_{20}\ r_0^2)^2\big[(1-q)^2/3 - q(1-q)\overline{(r_n/r_0)^2} + q^2\,\overline{(r_n/r_0)^4} + q^2\ \overline{(r_n/r_0)^2}\ \big] \qquad (24)$$

Now subtracting Eq.(18) from Eq.(24) we finally obtain

$$\sigma_w^2 = \overline{W^2} - \overline{W}^2 = (W_{20}\ r_0^2\ )^2\ [\ q^2\ r_{ms} + q^2\ \sigma_r^2 + (1-q)^2/12] \qquad (25)$$

where

$$r_{ms} = \overline{(r_n/r_0)^2} \qquad (26)$$

is the normalized mean square radius of the subaperture array, and

$$\sigma_r^2 = \overline{(r_n/r_0)^4} - \overline{(r_n/r_0)^2}^{\,2} = \overline{(r_n/r_0)^4} - r_{ms}{}^2 \qquad (27)$$

is the variance in the square of the subaperture radial position about that mean square radius.

Equation (25) appeared without derivation as Eq.(6-17) in the report and provides a great deal of insight into the behavior of phased arrays of telescopes which exhibit field curvature.

APPENDIX E

This Appendix provides a listing of the computer program used for numerically calculating the Strehl ratio versus field angle and its sensitivity to subaperture diameter for phased arrays of identical independent telescopes exhibiting various off-axis aberrations. Also shown is the tabulated and graphical output for comparison with the other techniques.

```
PRINT "MERSENNE-NUM(0; Dn)": PRINT

REM   This program is intended to compare the performance (Strehl ratio)
REM   versus field angle of different phased telescope array configurations
REM   where each telescope is a two-mirror afocal (Mersenne) design.  It is
REM   set up to plot families of curves for different subaperture diameters."

DIM  X0(20),Y0(20),E(110),E1(50),Y9(50)
PI  =  3.141592654#

REM    **********************    INPUT   DATA   *************************
PRINT "CHOOSE THE DESIRED TELESCOPE APERTURE CONFIGURATION, AND THE."
PRINT "ASSOCIATED DILUTION RATIO (RELATIVE SEPARATION IN SUBAPERTURE DIAMETE
RS)."
PRINT "  1.  MONOLITH"
PRINT "  2.  NNTT"
PRINT "  3.  MMT"
PRINT "  4.  GOLAY-6"
PRINT "  5.  MILLS CROSS"
PRINT "  6.  GOLAY-9"
PRINT "  7.  CIRCLE-N"
PRINT "  8.  OTHER"
INPUT Q,B
GOSUB 800

350 PRINT "INPUT TELESCOPE MAGNIFICATION,AND THE PRIMARY MIRROR F/NO."
INPUT M7,F8:  PRINT
PRINT "INPUT THE RANGE OVER WHICH YOU WANT THE DATA DISPLAYED"
PRINT "(IN MIN OF ARC), AND THE INCREMENT."
INPUT TMAX, DELT
L = .5: REM L = WAVELENGTH IN MICRONS
GOSUB 900

REM   *************CALCULATE  AND  PLOT  STREHL  RATIO  **************
LPRINT "MERSENNE-NUM. (; Dn)": LPRINT
ON Q GOTO  402,403,404,405,406,407,408,409
402 LPRINT"MONOLITH": GOTO 410
403 LPRINT"NNTT CONFIGURATION": GOTO 410
404 LPRINT"MMT CONFIGURATION": GOTO 410
405 LPRINT"GOLAY-6 CONFIGURATION": GOTO 410
406 LPRINT"MILL'S CROSS CONFIGURATION": GOTO 410
407 LPRINT"GOLAY-9 CONFIGURATION": GOTO 410
408 LPRINT"CIRCLE-";N;"  CONFIGURATION": GOTO 410
409 LPRINT "OTHER"
```

```
410 FOR D1 = .2 TO 1  STEP .2
LPRINT:LPRINT"Subaperture Diameter     = D =";D1;" Meters"
LPRINT "Primary  Mirror  F/No.     F =";F8
LPRINT "Telescope Magnification   = m =";M7
LPRINT "Dilution  Ratio           = B =";B
LPRINT "Wavelength                = L =";L;" Microns"

Q2 = 1: Q9 = 0
K9  =  2000000!*PI/L

REM *** SCALE SEPARATION ***
410 FOR J = 1 TO N
XN(J) = X0(J) * D1*B: YN(J) = Y0(J) * D1*B
RN(J) = SQR(XN(J)^2 + YN(J)^2)
NEXT J
R E M     ***********************
LPRINT:LPRINT TAB(0)"FIELD ANGLE";TAB(17)"VARIANCE";TAB(30)"STREHL RATIO"
CALL MOVETO (X1,Y1)
FOR T0 = 0 TO TMAX STEP DELT
IF T0 = 0 THEN 700
T1  =  T0  *  .000290888#
W2  =  (D1*(1-M7)/(16*F8*M7))*T1^2
W2  =  1000*1000*W2/L
A = 0: W = 0: WSQR = 0
FOR J = 1 TO N

FOR X3 = -1 TO 1.0001 STEP .2
FOR Y3 = -1 TO 1.0001 STEP .2
R3 = SQR(X3^2 + Y3^2)
IF R3 > 1.0001 THEN 460
A = A + 1
X = X3 * D1/2: Y = Y3 * D1/2
R = SQR(X^2 + Y^2)
XP = XN(J) + X: YP = YN(J) + Y
RP = SQR(XP^2 + YP^2)
WP = W2* R^2
W = W + WP
WSQR = WSQR + WP^2
460 NEXT Y3
NEXT X3

IF J > 1 THEN 470
MSQR = WSQR/A: SQRM = (W/A)^2
VAR = MSQR - SQRM
470 NEXT J
```

```
MSQR = WSQR/A: SQRM = (W/A)^2
VAR = MSQR - SQRM
RMS = SQR(VAR)
ARG = (2*PI)^2*VAR
SR = EXP(-ARG)
LPRINT TAB(5)T0;TAB(15)VAR;TAB(30)SR
IF SR < .4 THEN 730
GOTO 710
700 SR = 1
710 T8 = X1 + (X9-X1)*T0/TMAX
Z8 = Y9 - (Y9-Y1)*SR
CALL LINETO (T8,Z8)
720 NEXT T0

730 CALL MOVETO (T8-20,Z8+10):PRINT "D =";D1
NEXT D1

PICTURE OFF
OPEN "CLIP:PICTURE" FOR OUTPUT AS 1
PRINT #1, PICTURE$
CLOSE #1
END

W2* RN(J)^2 - 2*W2*(XN(J)*XP + YN(J)*YP)


800 REM **** SUBROUTINE TO CALCULATE SUBAPERTURE COORDINATES ****
ON Q GOTO 805,810,815,820,825,830,835,840
REM ****** MONOLITH ******
805 N = 1
X0(1) = 0: Y0(1) = 0
REM *********************
GOTO 850
REM ******** NNTT ********
810 N = 4
B3 = .707
X0(1) =   0 : Y0(1) = B3
X0(2) =  B3 : Y0(2) = 0
X0(3) =   0 : Y0(3) = -B3
X0(4) = -B3 : Y0(4) = 0
REM *********************
GOTO 850
REM ******** MMT *********
815 N = 6
```

```
B3 = .8660254
X0(1) =    .5 : Y0(1) = B3
X0(2) = 1     : Y0(2) = 0
X0(3) =    .5 : Y0(3) = -B3
X0(4) =   -.5 : Y0(4) = -B3
X0(5) = -1    : Y0(5) = 0
X0(6) =   -.5 : Y0(6) = B3
REM     **********************
GOTO 850
REM  ******  GOLAY-6  ********
820 N = 6
B3 = .8660254
X0(1) =  0    : Y0(1) =   1.5*B3
X0(2) =  1    : Y0(2) =   1.5*B3
X0(3) =     1 : Y0(3) =   -.5*B3
X0(4) =    .5 : Y0(4) = -1.5*B3
X0(5) = -1    : Y0(5) =   -.5*B3
X0(6) = -1.5 : Y0(6) =     .5*B3
REM     ************************
GOTO 850
REM  ******MILLS  CROSS  *******
825 N = 8
X0(1) =   0 : Y0(1) =   3
X0(2) =   0 : Y0(2) =   2
X0(3) =   3 : Y0(3) =   0
X0(4) =   2 : Y0(4) =   0
X0(5) =   0 : Y0(5) = -3
X0(6) =   0 : Y0(6) = -1
X0(7) = -3 : Y0(7) =   0
X0(8) = -1 : Y0(8) =   0
REM     ************************
GOTO 850
REM  ********  GOLAY-9  ********
830 N = 9
B3 = SQR(3)
X0(1) =  1.5 : Y0(1) =   1.25*B3
X0(2) =  1.5 : Y0(2) =     .25*B3
X0(3) =  2.5 : Y0(3) =     .25*B3
X0(4) =  1    : Y0(4) = -1.25*B3
X0(5) = -.5   : Y0(5) = -  .75*B3
X0(6) = -1    : Y0(6) = -1.25*B3
X0(7) = -2.5 : Y0(7) =     .25*B3
X0(8) = -1    : Y0(8) =     .75*B3
X0(9) = -1.5 : Y0(9) =   1.25*B3
REM     ************************
```

```
GOTO 850
REM  *********  CIRCLE-N  *********
835 PRINT"INPUT NUMBER OF SUBAPERTURES."
INPUT N
PHI = 2*PI/N
R = 1/(2*SIN(PHI/2))
FOR J = 1 TO N
PH = J * PHI
X0(J) = R*COS(PH)
Y0(J) = R*SIN(PH)
NEXT J
REM     *****************************
GOTO 850
REM  **********  OTHER  *********
840 PRINT "INPUT NUMBER OF SUBAPERTURES"
INPUT N
PRINT "INPUT X AND Y COORDINATE OF EACH SUBAPERTURE (RETURN), ETC."
FOR J = 1 TO N
INPUT  X0(J),Y0(J)
NEXT J
850  RETURN: REM     *********************************************

900 REM  *************  SUB  ROUTINE  TO  PLOT  AXES  *******************
REM *** X1 TO X9 IS RANGE OF ABSISSA
REM *** Y1 T0 Y9 IS RANGE OF ORDINATE
901 X1 = 70: X9 = 470
Y1 = 10: Y9 = 250
CLS
PICTURE ON
CALL SHOWPEN
REM  ******  PLOT  LINEAR  AXES  ******
LINE(X1,Y1)-(X9,Y9),,B
FOR K = 0 TO 10
LINE  (X1,Y1+(Y9-Y1)/10*K)-(X1+3,Y1+(Y9-Y1)/10*K)
LINE  (X9,Y1+(Y9-Y1)/10*K)-(X9-3,Y1+(Y9-Y1)/10*K)
NEXT K
FOR K = 0 TO 10 STEP 2
K7 = 1 - K/10
CALL MOVETO  (X1-25,15+(Y9-Y1)/10*K)
PRINT USING  "#.#";K7
NEXT K
K1 = (X9-X1)/(5*TMAX)
FOR K = X1 TO X9 STEP K1
LINE  (K,Y1)-(K,Y1+3)
LINE  (K,Y9)-(K,Y9-3)
```

```
NEXT K
K7 = -1
FOR K = X1 TO X9 STEP (X9-X1)/TMAX
LINE (K,Y1)-(K,Y1+6)
LINE (K,Y9)-(K,Y9-6)
K7 = K7 +1
CALL MOVETO (X1-9+K7*(X9-X1)/TMAX,Y9+16)
PRINT USING "##";K7
NEXT K
X8 = (X9+X1)/2-75
CALL MOVETO (X8, Y9+30)
PRINT"FIELD ANGLE (ARC MIN)"
Y = Y1 + 25
FOR K = 1 TO 13
READ LAB$
Y = Y + 12
CALL MOVETO (X1-40,Y)
PRINT LAB$
NEXT K
DATA S,T,R,E,H,L, , ,R,A,T,I,O
FOR J = 1 TO N
X7(J) = 130 + 20*X0(J)*B:  Y7(J) = 200 + 20*Y0(J)*B
CIRCLE(X7(J),Y7(J)),10
NEXT J
CALL MOVETO (220,190)
PRINT "Wavelength =";L;" Microns"
CALL MOVETO (220,205)
PRINT"Primary Mirror F/No. =";F8
CALL MOVETO (220,220)
PRINT"Telescope Magnification = ";M7
CALL MOVETO (220,235)
PRINT"Dilution Ratio = ";B
RETURN
REM     ****************************
```

```
MERSENNE-NUM. (θ; Dn)

MONOLITH

Subaperture Diameter        = D = .2  Meters
Primary  Mirror  F/No.        F = 2.5
Telescope Magnification     = m = .1
Dilution  Ratio             = B = 1.2
Wavelength                  = L = .5  Microns

FIELD ANGLE       VARIANCE        STREHL RATIO
     1          5.366996E-10      1
     2          8.587193E-09      .9999996
     3          4.347264E-08      .9999983
     4          1.373951E-07      .9999946
     5          3.354386E-07      .9999868
     6          6.955622E-07      .9999725
     7          1.288616E-06      .9999492
     8          2.198321E-06      .9999132
     9          3.521292E-06      .999861
     10         5.367017E-06      .9997882
     11         7.85784E-06       .9996898
     12         1.1129E-05        .9995607
     13         1.532866E-05      .999395
     14         2.061786E-05      .9991864
     15         2.717044E-05      .998928

Subaperture Diameter        = D = .4  Meters
Primary  Mirror  F/No.        F = 2.5
Telescope Magnification     = m = .1
Dilution  Ratio             = B = 1.2
Wavelength                  = L = .5  Microns

FIELD ANGLE       VARIANCE        STREHL RATIO
     1          3.434877E-08      .9999986
     2          5.495804E-07      .9999783
     3          2.782249E-06      .9998901
     4          8.793286E-06      .9996529
     5          2.146807E-05      .9991528
     6          4.451598E-05      .9982441
     7          8.247141E-05      .9967495
     8          1.406926E-04      .9944611
     9          2.253627E-04      .9911425
     10         3.434891E-04      .9865311
     11         5.029017E-04      .980342
     12         7.122557E-04      .9722729
     13         9.810342E-04      .9620107
     14         1.319543E-03      .9492401
     15         1.738909E-03      .933654
```

Subaperture Diameter = D = .6 Meters
Primary Mirror F/No. F = 2.5
Telescope Magnification = m = .1
Dilution Ratio = B = 1.2
Wavelength = L = .5 Microns

FIELD ANGLE	VARIANCE	STREHL RATIO
1	3.912543E-07	.9999846
2	6.260065E-06	.9997529
3	3.169163E-05	.9987497
4	1.00161E-04	.9960536
5	2.445337E-04	.9903926
6	5.070661E-04	.9801809
7	9.394006E-04	.9635932
8	1.602578E-03	.9386926
9	2.567025E-03	.9036239
10	3.91254E-03	.856877
11	5.72836E-03	.7976012
12	8.113056E-03	.725938
13	1.117459E-02	.6432928
14	1.503041E-02	.5524585
15	.0198073	.457508

Subaperture Diameter = D = .8 Meters
Primary Mirror F/No. F = 2.5
Telescope Magnification = m = .1
Dilution Ratio = B = 1.2
Wavelength = L = .5 Microns

FIELD ANGLE	VARIANCE	STREHL RATIO
1	2.198321E-06	.9999132
2	3.517314E-05	.9986124
3	1.78064E-04	.992995
4	5.627703E-04	.9780277
5	1.373956E-03	.9472032
6	2.849024E-03	.8936197
7	5.278174E-03	.8119034
8	9.004325E-03	.7008394
9	.0144232	.5658619
10	.0219833	.4198466
11	3.218569E-02	.2806519

Subaperture Diameter = D = 1 Meters
Primary Mirror F/No. F = 2.5
Telescope Magnification = m = .1
Dilution Ratio = B = 1.2
Wavelength = L = .5 Microns

FIELD ANGLE	VARIANCE	STREHL RATIO
1	8.38595E-06	.999669
2	1.341752E-04	.994717
3	6.792608E-04	.9735402
4	2.146803E-03	.9187397
5	5.241212E-03	.813089
6	1.086817E-02	.651122
7	2.013465E-02	.4516336
8	3.434885E-02	.2576796

NUMERICAL CALCULATION (q = 0)

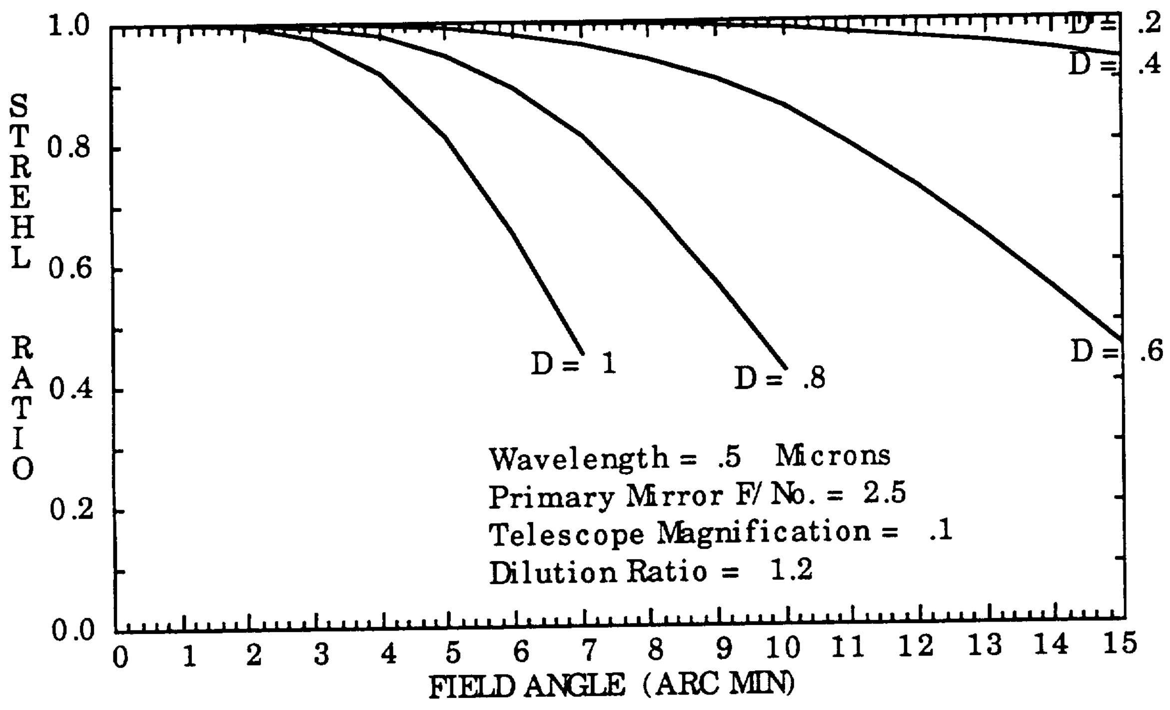

This graph should be compared to the Strehl ratio predicted from the analytical solution for wavefront variance illustrated in Figure 6-14 of this report.